Space Sci Rev (2009) 146: 295–327
DOI 10.1007/s11214-009-9497-6

Physics of the Solar Wind–Local Interstellar Medium Interaction: Role of Magnetic Fields

G.P. Zank · N.V. Pogorelov · J. Heerikhuisen · H. Washimi · V. Florinski · S. Borovikov · I. Kryukov · H.R. Müller

Received: 3 November 2008 / Accepted: 19 February 2009 / Published online: 7 May 2009

Abstract The interaction of the solar wind with the local interstellar medium is characterized by the self-consistent coupling of solar wind plasma, both upstream and downstream of the heliospheric termination shock, the interstellar plasma, and the neutral atom component of interstellar and solar wind origin. The complex coupling results in the creation of new plasma components (pickup ions), turbulence, and anomalous cosmic rays, and new populations of neutral atoms and their coupling can lead to energetic neutral atoms that can be detected at 1 AU. In this review, we discuss the interaction and coupling of global sized structures (the heliospheric boundary regions) and kinetic physics (the distributions that are responsible for the creation of energetic neutral atoms) based on models that have been developed by the University of Alabama in Huntsville group.

Keywords Solar wind boundaries · Interstellar medium · Pickup ions · Energetic neutral atoms

1 Introduction

In the last two decades, great progress has been made in our understanding of the physical processes thought to describe the outer heliosphere. Fundamental to these advances has been the recognition that the interstellar medium is coupled intimately to the heliosphere through a variety of mechanisms and that much of outer heliospheric physics cannot be understood independently of the local interstellar medium (LISM). As a result, this field truly lies at the crossroads of space physics and astrophysics. For the first time, *in situ* measurements by the spacecraft Voyager 1 (V1), Voyager 2 (V2) and remote sensing observations by IBEX will allow us to directly probe the boundaries of the solar wind–LISM interaction region, and will provide data of unprecedented quality about the nature of the interstellar medium.

G.P. Zank (✉) · N.V. Pogorelov · J. Heerikhuisen · H. Washimi · V. Florinski · S. Borovikov · I. Kryukov · H.R. Müller
Center for Space and Aeronomic Research (CSPAR) and Department of Physics, University of Alabama, Huntsville, AL, USA
e-mail: zank@cspar.uah.edu

Voyager 1 crossed the termination shock (TS) of the supersonic flow of the solar wind on 16 December 2004 at a distance of 94 astronomical units (AUs) from the Sun, becoming the first spacecraft to enter the heliosheath (Stone et al. 2005; Burlaga et al. 2005; Decker et al. 2005; Gurnett and Kurth 2005). Voyager 2 crossed the heliospheric TS several times between 30 August and 1 September 2007 (Stone et al. 2008; Richardson et al. 2008; Burlaga et al. 2008; Decker et al. 2008; Gurnett and Kurth 2008), at a distance of 84 AU, providing the first plasma measurements of the TS and heliosheath region. With IBEX, we are poised at the threshold of an exciting decade of new observations of the heliosheath boundaries that will provide not only information about the boundaries and the plasma regimes in which energetic neutral atoms (ENAs) are created, but will be able to provide this information on a global scale. The IBEX mission will provide new and unexpected insights into the solar wind and the LISM, as well as into the stellar winds of neighboring stars and their LISM.

The heliosphere is the region of space filled by the expanding solar corona; a vast region indeed extending perhaps 150–180 AUs in the direction of the Sun's motion through the interstellar medium and several thousand AU in the opposite direction. A convenient, if slightly vague, definition of the outer heliosphere, and one that we adopt here, is that it is that region of the solar wind influenced dynamically by physical processes associated with the LISM. Thus, for example, neutral interstellar hydrogen (H) is the dominant (by mass) constituent of the solar wind beyond an ionization cavity of ∼6–10 AUs in the upstream direction (the direction antiparallel to the incident interstellar wind). The neutral H is coupled weakly to the solar wind plasma via resonant charge exchange—a coupling that leads to the creation of pickup ions that come to eventually dominate the internal energy of the solar wind. The solar wind changes then from a small plasma beta β_{SW} (the ratio of plasma pressure to magnetic field pressure) environment to one in which $\beta_{SW} \simeq 4$. As a by-product of the creation of pickup ions, low-frequency turbulence is generated, replenishing the dissipated magnetic fluctuations originating at and near the Sun (Williams and Zank 1994; Zank et al. 1996a). This has important implications for both solar wind heating and charged particle transport (Williams et al. 1995; Zank et al. 1998). Our growing understanding of the physical processes governing the outer heliosphere has led to major discoveries about both our own solar system (the discovery of a "hydrogen wall" bounding our heliosphere, for example (Linsky and Wood 1996; Gayley et al. 1997), the interstellar medium (the composition of the ISM (Gloeckler and Geiss 1998)), and the astrospheres of other stars (such as the discovery of winds blown from stars like our Sun (Wood et al. 2001)). Since the Sun orbits our galactic center, the solar system has experienced many different interstellar environments, and it is entirely possible that this may have, and may have had, an important impact on the Earth's environment (Zank and Frisch 1999e; Scherer et al. 2001; Florinski et al. 2003b; Florinski and Zank 2006; Zank et al. 2006; Müller et al. 2006; Scherer et al. 2008).

The physics underlying the interaction of the solar wind with the LISM describes a complex relationship between several basic elements: the solar wind plasma and magnetic field, the LISM plasma and magnetic field, the LISM neutrals, interstellar pickup ions, and anomalous and galactic cosmic rays. The solar wind terminates at a shock whose location is determined by the balance of dynamical solar wind pressure and the external LISM pressure (Davis 1955; Parker 1963; Axford 1972). Galactic cosmic rays, which can diffuse deep into the heliosphere, are of lesser dynamical importance. Interstellar neutral H is coupled to both the LISM and solar wind plasmas through resonant charge exchange, providing an effective volumetric force and hence affecting the dynamical nature of the solar wind–LISM interaction profoundly. The two basic ways in which neutrals can modify the he-

liospheric and LISM plasmas are: (i) Interstellar neutrals decelerate the solar wind indirectly; (ii) Secondary very hot neutrals produced in the shocked solar wind (downstream of the TS) can, through secondary charge exchange, heat the LISM, as can fast neutrals produced through charge exchange with the supersonic solar wind. Newly created ions in the supersonic solar wind—the pickup ions—are very energetic ($\sim$ 1 keV) compared to typical solar wind protons and dominate the internal energy of the solar wind in the outer heliosphere. The pickup process itself is expected to generate significant levels of low frequency magnetohydrodynamic (MHD) turbulence, which will isotropize the pick-up ion beam, dissipate and heat the solar wind and scatter cosmic rays (Williams et al. 1995; Matthaeus et al. 1999; Smith et al. 2000; Zank et al. 1996b; Isenberg et al. 2003; Zank et al. 1998). Some small fraction of the pickup ions will be further energized and, possibly at the TS (although this remains a mystery despite, or perhaps because of, the recent Voyager crossings of the TS), be accelerated up to MeV energies to form the anomalous cosmic-ray (ACR) component. The energy density of the anomalous cosmic rays in the vicinity of the TS was expected to modify the structure and properties of the shock itself. Present day models hope to capture the fully non-linear coupled physics of the solar wind–LISM interaction, and progress has been made at several levels of approximation. The most comprehensive models today are fully 3D and time-dependent, and include solar wind and LISM plasma and magnetic fields at an MHD level, and are coupled self-consistently with interstellar neutral H at either a kinetic or multi-fluid level. Many key parameters remain nonetheless somewhat poorly constrained, particularly properties of the LISM such as the magnetic field strength and orientation and the ionization fraction.

Besides helping explain the observations returned by the Voyager spacecraft, an understanding of the plasma downstream of the TS, the inner heliosheath plasma, is critical to interpreting observations that will be made by the IBEX mission. IBEX (McComas et al. 2006) will measure ENAs at 1 AU that are created by charge exchange between interstellar neutral atoms of low energy and inner heliosheath plasma. The working assumption is that the heliosheath plasma will be very hot (model temperatures suggest $\sim 10^6$ K). An observational (if not entirely theoretical) surprise was the discovery by V2 (Richardson et al. 2008) that only 20% of the incident solar wind flow energy went into heating the solar wind ions, making them a relatively cool component of the downstream shocked inner heliosheath plasma (to the extent that the downstream flow appears to be supersonic, at least as determined from solar wind ions!). As we shall discuss, the form of the heliosheath distribution function can make a profound difference in the measured ENA distribution. Heerikhuisen et al. (2008a) find significant differences in the ENA distribution resulting from assuming either a Maxwellian or a kappa (κ) distribution for the solar wind ions in the heliosheath. Undoubtedly, since the downstream or heliosheath plasma distribution is determined by the processing of the supersonic solar wind by the TS, a cold solar wind ion heliosheath component will have an important impact on interpreting the IBEX ENA measurements.

With the upcoming IBEX mission, it is appropriate to elucidate the basic physics underlying models that describe the self-consistent interaction of the solar wind with the LISM. IBEX will return all-sky maps and distributions integrated over lines-of-sight, and the deconvolution and interpretation of these observations will rely heavily on complementary modeling. IBEX will undoubtedly return data that taxes both our models and the assumptions underlying them and we will need to understand the theory thoroughly. This review discusses the assumptions underlying the most sophisticated models that we currently possess—a fully 3D time-dependent model that incorporates solar and LISM plasma and magnetic fields with interstellar neutral H self-consistently (both kinetically and using a multi-fluid description). This review is based on two much more detailed

and lengthy discussions of the interaction of the solar wind with the LISM (Zank 1999; Zank et al. 2008).

2 Mathematical Formulation for Modeling the Solar Wind–LISM Interaction

Key to understanding the structure and properties of the heliosphere is the effect that interstellar neutral gas, primarily hydrogen, plays in the physics of the solar wind–LISM interaction. Interstellar neutral gas flows into the heliosphere relatively unimpeded and can penetrate to within several AU of the sun. Neutral atoms scatter solar radiation resonantly so that the distribution of H and Helium (He) in the heliosphere can be studied by observing sky background radiation in HI $\lambda 1216$ and HeI $\lambda 584$. The distribution of interstellar H only is addressed here in any detail since He and the other elements have a negligible dynamical influence on the solar wind–LISM interaction. Nonetheless, He in particular provides important and direct information about the conditions in the LISM (Möbius et al. 2004; Witte 2004), such as the interstellar flow speed, direction, and temperature.

The heliospheric-LISM plasma environment is composed of three thermodynamically distinct regions: (i) the supersonic solar wind, expanding more-or-less radially from the Sun at speeds of $\sim$ 400–800 km/s, with a density that decays as $\sim r^{-2}$ (r denoting radial heliocentric distance from the Sun), and a relatively low temperature ($\sim 10^4$ K in the vicinity of the HTS) which appears to decay adiabatically with an effective adiabatic index of $\gamma \simeq 1.1$ within about 20 AU (see Williams et al. 1995; Matthaeus et al. 1999); (ii) the shock heated subsonic solar wind, which possesses much higher "effective" temperatures ($\sim 10^6$ K), somewhat higher densities ($\sim 10^{-3}$ cm^{-3}) and lower flow speeds ($\sim$ 100 km/s); and finally (iii) the LISM, where the plasma flow speed is low ($\sim$ 26 km/s) and the temperature is several $\times 10^3$K. Here and henceforth, region 1 is taken to be the region beyond the heliopause (HP) i.e., the LISM, and H atoms whose origin lies in region 1 shall be referred to as component 1 neutrals. One can further subdivide the LISM region into a possibly shocked region (if a bow shock exists), region 1b, and an unshocked region, region 1a. Region 2 is that region occupied by the shocked solar wind, plasma and component 2 neutrals are those created in region 2. Finally, region 3 refers to the supersonic solar wind, and the component 3 neutrals are those born there (i.e., the "splash" component). Quite clearly, the neutral populations, components 1a, 1b, 2 and 3, possess distinct characteristics, and the complete local neutral H distribution will be highly anisotropic.

Several interactions between H atoms, protons and electrons are possible and some important points can be made (Zank 1999). (1) Photoionization is important within several AU, but is otherwise not (assuming that the LISM is in ionization equilibrium with the local stellar UV radiation field, as suggested (Frisch 1995); see also Slavin and Frisch (2002). (2) Two charge-exchange cross-sections are used in the literature (Maher and Tinsley 1977; Fite et al. 1962; Maher and Tinsley 1977; Fite et al. 1962), but that published by Fite et al. (1962) is a fit to experimental data. Nonetheless, at 1 eV, a 40% discrepancy exists between the cross-sections and this can effect the heliospheric H number density by a similar amount. However, the cross-sections provided by Lindsay and Stebbings (2005) are now regarded as the "accepted" values. (3) The charge-exchange cross-sections assume that no momentum transfer occurs during the interaction but, of course, non-charge-exchange H^+–H interactions can occur. The H^+–H cross-section computed by Dalgarno (1960) is the total momentum transfer cross-section and includes charge-exchange. Thus, an exclusively charge-exchange treatment of the H–H^+ interaction may underestimate the efficiency of the coupling. (4) H–H collisions have a cross-section comparable to that of charge-exchange. It

is presently unclear how and where such collisions may be important, but two possibilities are in the heliotail and the region upstream of the HP where hot component 2 and cooler component 1 neutrals can equilibrate Williams et al. (1997). (5) Electron-H collisions, electron impact ionization, and recombination are unlikely to be dynamically important on 1000 AU scales. However, because electron impact ionization is sensitive to the electron distribution, it may occur in the solar wind (Isenberg and Feldman 1995). (6) Since region 1 H^+–H^+ and e–e mean free paths are ~ 0.15 AU, the LISM is Coulomb collisional and the electrons equilibrate to the proton temperature.

The distribution of neutral H, both LISM and that created in the various boundary regions of the heliosphere, drifting through the heliosphere may be calculated directly from the Boltzmann equation,

$$\frac{\partial f}{\partial t} + \mathbf{v} \cdot \nabla f + \left(\frac{\mathbf{F}}{m} \cdot \nabla_{\mathbf{v}} \right) f = P - L, \tag{1}$$

where $f(\mathbf{x}, \mathbf{v}, t)$ is the neutral H particle distribution function expressed in terms of position $\mathbf{x}$, velocity $\mathbf{v}$ and time t. $\mathbf{F}$ is the force acting on a particle of mass m, typically gravity and radiation pressure. The terms P and L describe the production and loss of particles at $(\mathbf{x}, \mathbf{v}, t)$, and both terms are functions of the assumed plasma and neutral distributions. In all cases of interest here, the loss term may be expressed as

$$L = f(\mathbf{x}, \mathbf{v}, t)\beta(\mathbf{x}, \mathbf{v}, t), \tag{2}$$

where β is the total loss rate in s^{-1}. The neutral H loss rate due to charge-exchange is obtained by integrating over the proton distribution function, thus

$$\beta_{ex}(\mathbf{x}, \mathbf{v}, t) = \int f_p(\mathbf{x}, \mathbf{v}_p, t) V_{rel,p} \sigma_{ex}(V_{rel,p}) \mathrm{d}^3\mathbf{v}_p, \tag{3}$$

where f_p and $\mathbf{v}_p$ refer to proton quantities, $V_{rel,p} \equiv |\mathbf{v} - \mathbf{v}_p|$ is the relative speed between an H atom and a proton, and σ_{ex} denotes the charge-exchange cross-section.

The charge-exchange neutral H production term is given by

$$P_{ex}(\mathbf{x}, \mathbf{v}, t) = f_p(\mathbf{x}, \mathbf{v}, t) \int f_H(\mathbf{x}, \mathbf{v}_H, t) V_{rel,H} \sigma_{ex} \left(V_{rel,H} \right) \mathrm{d}^3\mathbf{v}_H, \tag{4}$$

where $V_{rel,H} \equiv |\mathbf{v} - \mathbf{v}_H|$ and f_H is the neutral H distribution.

The initial or boundary data is assumed typically to be a Maxwellian distribution parameterized by the bulk LISM density, velocity and temperature, and the boundary condition is imposed at "infinity".

All models of the solar wind interaction with the LISM assume a simple model of the plasma which incorporates both a solar wind component and a suprathermal component. Although number densities are too low for the direct interaction of the solar wind plasma flow with the neutral flux, appreciable momentum and energy exchange, particularly in the supersonic solar wind, is possible nonetheless through charge exchange of solar wind protons and neutral H. In a plasma possessing a sufficiently strong magnetic field, a newly charged particle acquires a gyrospeed equal to its initial velocity relative to the plasma and convects with the plasma flow within a gyroperiod. Although the microscopic details of this process are complicated and depend on the plasma-magnetic field configuration (Williams and Zank 1994; Isenberg and Lee 1996; Zank 1999), the net result of ion pickup on hydrodynamic scales is qualitatively unique—there is a change in the density, momentum, and energy of the plasma flow for each act of charged particle production or destruction.

The dynamical or ram pressure (ρu^2) and thermal pressure p of the solar wind decrease with increasing heliocentric distance and must reach a value which eventually balances the pressure exerted by the LISM. The relaxation towards pressure equilibrium between the solar and interstellar plasmas is characterized by (i) a transition of the supersonic solar wind flow to a subsonic state, and (ii) a divergence of the interstellar flow about the heliospheric obstacle. The transition of the supersonic solar wind is accomplished by means of a shock transition, the TS. Voyager 1 has now crossed the TS (at 94 AU) (Stone et al. 2005; Burlaga et al. 2005) and V2 crossed at 84 AU (Stone et al. 2008; Richardson et al. 2008; Burlaga et al. 2008). The divergence of the LISM flow about the heliosphere may be accomplished either adiabatically (if the relative motion between the Sun and the LISM is subsonic) or by means of a bow shock in the case of supersonic relative motion. Although one can estimate the location of the TS and the HP, the discontinuity separating solar wind material from the interstellar plasma (a contact/tangential discontinuity in the case of gas/MHD), using simple pressure balance arguments, the problem of the interaction of the solar wind with the LISM is fundamentally multi-dimensional. Thus, the main advances in our understanding of global heliospheric structure since the pioneering work of Davis (1955), Parker (1958, 1961, 1963), Axford et al. (1963) and Baranov et al. (1971) have been more recent and based largely on computer simulations. The initial simulations were based on pure one-fluid gas dynamic models, but now the self-consistent inclusion of neutral interstellar hydrogen models is recognized as the key to understanding the structure and properties of the large-scale heliosphere. We discuss the basic MHD model, and the kinetic and multi-fluid approaches to including neutral H self-consistently in heliospheric models of the solar wind–LISM interaction.

Interplanetary and interstellar magnetic fields have only recently been fully incorporated into global heliospheric models. The most detailed models (fully 3D and time-dependent and including neutral H both kinetically and in the multi-fluid approximation—see below) are those described here and developed by the University of Alabama in Huntsville group. To model the interaction of the solar wind with a partially ionized LISM, the following 3D set of MHD equations must be solved,

$$\frac{\partial \rho}{\partial t} + \nabla \cdot \rho \mathbf{u} = Q_\rho; \tag{5}$$

$$\rho \frac{\partial \mathbf{u}}{\partial t} + \rho \mathbf{u} \cdot \nabla \mathbf{u} + (\gamma - 1) \nabla e + (\nabla \times \mathbf{B}) \times \mathbf{B} = \mathbf{Q}_m; \tag{6}$$

$$\frac{\partial}{\partial t} \left(\frac{1}{2} \rho u^2 + e + \frac{B^2}{8\pi} \right) + \nabla \cdot \left[\left(\frac{1}{2} \rho u^2 + \gamma e \right) \mathbf{u} + \frac{1}{4\pi} \mathbf{B} \times (\mathbf{u} \times \mathbf{B}) \right] = Q_e; \tag{7}$$

$$\frac{\partial \mathbf{B}}{\partial t} - \nabla \times (\mathbf{u} \times \mathbf{B}) = 0; \tag{8}$$

$$\nabla \cdot \mathbf{B} = 0, \tag{9}$$

$\rho = m_p n$, together with the equation of state $e = \alpha n k_B T/(\gamma - 1) = p/(\gamma - 1)$. Here the choice of $\alpha = 2$ (or greater if incorporating the contribution of cosmic rays, dust indirectly) corresponds to a plasma population comprising electrons and protons. The remaining variables have their usual definitions, and the source terms Q_ρ, $\mathbf{Q}_m$, and Q_e serve to couple the neutral H and proton populations. Certain subtleties in the formulation of an MHD model

in the presence of neutral H need to be recognized, and this was discussed by Florinski and Zank (2003d) in the context of non-ideal MHD. Subject even to the assumption of an isotropic solar wind, the formulation (5)–(9) is inherently 3D thanks to the solar magnetic field and the current sheet.

As discussed, pickup ions are created in the solar wind through charge-exchange of LISM neutrals with solar wind protons, but they do not thermalize with the background solar wind plasma (Isenberg 1986; Zank 1999) and are not therefore equilibrated with the solar wind. Pickup ions constitute a separate suprathermal particle population in the SW (Möbius et al. 1985; Gloeckler et al. 1993; Gloeckler 1996; Gloeckler and Geiss 1998) and contribute to the power-law tails observed almost universally in the solar wind plasma distribution (Mewaldt et al. 2001; Fisk and Gloeckler 2006). Heerikhuisen et al. (2008a) and Prested et al. (2008) suggested that a simple way to incorporate a power-law tail, and thereby model the proton, energetic particle, and pickup ion populations as a single distribution, is to assume a generalized Lorentzian, or κ-, distribution (Bame et al. 1967; Summers and Thorne 1991; Collier 1995) given by

$$f_p(\mathbf{v}) = \frac{n_p}{\pi^{3/2}\theta_p^3}\frac{1}{\kappa^{3/2}}\frac{\Gamma(\kappa+1)}{\Gamma(\kappa-1/2)}\left[1+\frac{1}{\kappa}\frac{(\mathbf{v}-\mathbf{u})^2}{\theta_p^2}\right]^{-(\kappa+1)}, \tag{10}$$

where θ_p is a typical speed related to the effective temperature of the distribution, and is evaluated using the pressure moment, discussed further below. The distribution function (10) possesses a Maxwellian core, a power-law tail that scales as $v^{-2(\kappa+1)}$, and reduces to a Maxwellian in the limit of large κ. Although the core and tail features agree qualitatively with observations, a limitation of the κ formalism is that it does not allow for the relative abundances of core and tail to be adjusted for a particular choice of κ. Obviously, the observed flat-topped pickup ion population is also absent in the κ approximation. In Fig. 1, we plot a κ-distribution for $\kappa = 1.63$, comparing it to a Maxwellian distribution (Heerikhuisen et al. 2008a).

As recognized by Heerikhuisen et al. (2008a), the MHD equations for the plasma do not change if a κ-distribution for the solar wind protons is assumed—this is because the basic fluid conservation laws do not assume a specific form of the distribution function (see for example Burgers 1969). Closure at the second moment is possible if the distribution is isotropic, since the heat flux and the off-diagonal components of the stress tensor are then identically zero. The only difference from conventional fluid dynamics is that the collision integrals do not vanish as they would for a Maxwellian distribution. However, collisional frequencies are so low for the SW that we may neglect these collisional terms and treat the distribution function (10) as "frozen" into the plasma. Even though the solar wind is effectively collisionless, an MHD approach is still warranted since the plasma has fluid properties perpendicular to the magnetic field, while various wave phenomena help isotropize the distribution (see for example Khabibrakhmanov et al. 1996; Kulsrud 1984). For these reasons, Heerikhuisen et al. (2008a) solve the regular MHD equations to determine the bulk plasma quantities, but in the inner heliosheath they interpret these as having come from (10). For simplicity, Heerikhuisen et al. assume $\kappa = 1.63$ for the solar wind plasma, which is a value consistent with the data analysis of Decker et al. (2005). We may anticipate that observations by the IBEX mission can be used to estimate or constrain κ in the heliosheath, and we follow the discussion by Heerikhuisen et al. (2008a) to indicate how this can be done.

The κ distribution is an approximation in the sense that it is relatively straightforward to include a tail on the plasma distribution, which emerges directly from a thermal core.

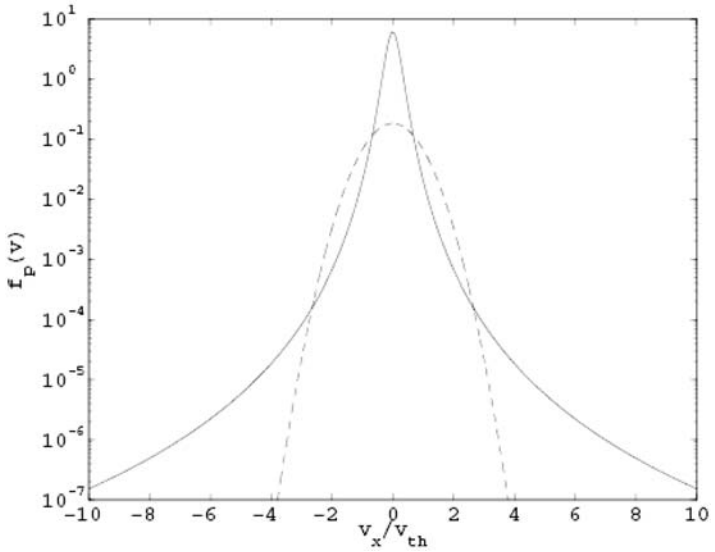

Fig. 1 A 1D cut of the velocity distribution function in the plasma frame for $\kappa = 1.63$ (*solid line*), together with a Maxwellian distribution (*dashed line*). Note that the core of the κ-distribution is narrower than the Maxwellian, but the zeroth and second moments are the same for both distributions. Here, we have defined $v_{th} = \theta_p\sqrt{\kappa/(\kappa - 3/2)}$—see (12). Heerikhuisen et al. (2008a)

In this, it mimics the pickup ion distribution. However, the core and tail of a κ distribution are coupled self-similarly, meaning that broadening of the core leads to a corresponding broadening of the tail, and this may not be a feature of separate pickup ion and thermal solar wind distributions. We note that the magnetic field orientation and solar wind speed are unlikely to have much effect on the overall pickup ion distribution. In principle, the subsequent scattering of the pickup ions shortly after birth onto (most probably) a bispherical distribution should wash out much of the initial magnetic field orientation characteristics, and the gradual cooling of the pickup ions, and thus creation of the filled shell distribution, is likely to weaken the dependence on solar wind flow speed. Thus, in summary, the κ distribution probably captures adequately the dynamic range of the pickup ion distribution and its underlying symmetry, but it introduces a coupling between the core distribution and the tail that may not accurately reflect the physics of a separate thermal solar wind core and pickup ion distribution.

The κ- and Maxwellian plasma distribution functions are linked through the choice of θ_p in equation for the isotropic plasma pressure. Thus, using

$$p = \frac{4\pi m_p}{3}\int_0^\infty v^4 f_p(v)dv = \frac{\rho\theta_p^2}{2}\frac{\kappa}{\kappa - 3/2}, \tag{11}$$

allows us to introduce an effective temperature for the κ-distribution as

$$T_{\rm eff} = \frac{p}{nk_B}, \tag{12}$$

so that

$$p = \frac{2k_B T_{eff}}{m_p}\frac{1}{\theta_p^2}\frac{\kappa - 3/2}{\kappa}.$$

Note the singularity $\kappa \longrightarrow 3/2$, which corresponds to a v^{-5} tail (Fisk and Gloeckler 2006) and an unbounded pressure.

As discussed above, for a Maxwellian distribution (Pauls et al. 1995) the charge exchange loss terms depend on the assumed proton distribution. For a κ-distribution, Heerikhuisen et al. follow a derivation analogous to that of Pauls et al. (1995) and Zank (1999) to find that the charge exchange loss rate is now given by

$$\beta_{ex} = n\sigma_{ex}\sqrt{\frac{4\Gamma^2(\kappa+1)\theta_p^2}{\pi\kappa(\kappa-1)\Gamma^2(\kappa-1/2)} + (\mathbf{v}-\mathbf{u})^2}, \tag{13}$$

which, in the limit of large κ i.e., a Maxwellian, reduces to distribution,

$$\beta_{ex} = n\sigma_{ex}\sqrt{\frac{4}{\pi}\theta_p^2 + (\mathbf{v}-\mathbf{u})^2}. \tag{14}$$

It is of interest that the Heerikhuisen et al. (2008a) approach has the consequence that the locations of the TS, HP and bow shock change when pickup ions react self-consistently on the plasma, a result that is consistent with the 5-fluid model of Fahr et al. (2000) that introduces PUIs as an explicit plasma component. This distinguishes the self-consistent approach from the "post-processing" approach used by Prested et al. (2007), and is discussed further below.

The mean free path for charge-exchange collisions can be very large in the heliospheric boundary regions and in the supersonic solar wind. To illustrate this point, we plot in Fig. 2 the average number of charge-exchange events per particle as a function of spatial location for a steady-state kinetic based simulation (Heerikhuisen et al. 2006a, 2006b; 2008a). The Sun is located at the origin. Clearly, the number of charge exchange events varies throughout the heliosphere and the solar wind–LISM boundary regions, with no more than two charge exchanges being typical for the region extending from beyond the nose of the HP to 500 AU from the Sun in the heliotail. Other regions can experience more charge exchange events; the flanks for example can have as many as 5 events per particle on average. Thus, ideally one should calculate the interstellar neutral distribution at a kinetic level since the Knudsen number $Kn \simeq 1$ for neutral H throughout large regions of the heliosphere, or recognize that a single set of gas dynamical equations cannot adequately describe the different neutral H populations created through charge exchange. However, a multiple set of gas dynamics equations corresponding to various neutral particle populations that are created in different thermodynamical regions of the heliosphere and LISM can be a good approximation to the fully kinetic description, subject to certain caveats.

Neutral H gas is coupled to the plasma through appropriate source terms. When a fluid description for the neutrals is assumed, source terms are calculated using approximations to integrals over the distribution functions convolved with the charge-exchange cross-section. Since the form of the distribution functions originating from all possible source regions is known at all points in time, the coupling between the codes can be done at every time-step for each species in the code. This gives rise to very tight, accurate coupling, so that both steady-state problems such as the one considered here, as well as fully dynamic problems, can be solved (Zank and Müller 2003; Florinski et al. 2005a).

Coupling a Monte-Carlo code to a plasma code is more difficult than the corresponding coupling to a multi-fluid model (Baranov and Malama 1993; Heerikhuisen et al. 2006). To avoid making assumptions about the nature of the distribution function, source terms for the

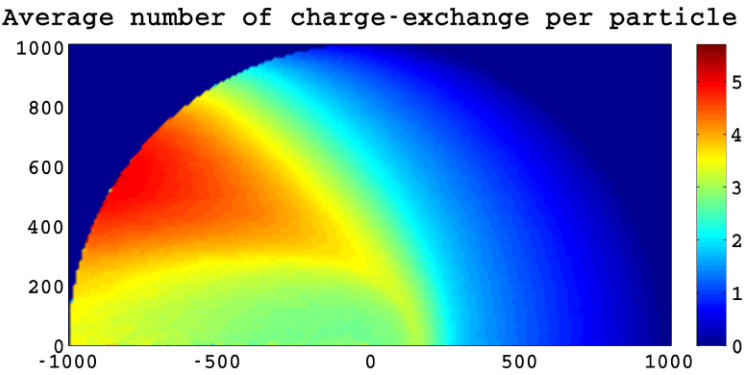

Fig. 2 The average number of charge-exchange events per particle as a function of spatial location for a steady-state model of the heliosphere interaction with the LISM. This simulation is based on a Monte-Carlo treatment (Heerikhuisen et al. 2006a, 2006b) of the kinetic neutral H, and is discussed further below. This figure illustrates the regions where the Knudsen number $Kn \simeq 1$. The distance along both axes is measured in AU, centered on the Sun (the origin)

plasma must be gathered in terms of individual charge-exchange events. Each event contributes to the plasma source at one location. It therefore requires a large number of charge-exchange events within each grid-cell in order to generate smooth and accurate sources for the plasma. When solving a steady-state problem, we may simply compute as many particle trajectories through the domain as is necessary for smooth sources. Time-dependent problems may be solved by collecting sources over a time interval which is shorter than the shortest time-scales we are trying to resolve. Under this constraint, we typically need a large number of particles to retain accuracy if the timescales present in the solution are small.

Extending the original hydrodynamic-like model of Baranov et al. (1981) and Baranov and Malama (1993, 1995) used a Monte-Carlo approach to solve the neutral H Boltzmann equation and coupled this self-consistently to a steady-state 2D hydrodynamic model of the solar wind and LISM plasma. The method of coupling is that of "global iterations". Here the plasma code is run to a steady-state iteratively, using the source term generated by running the neutrals on the preceding plasma state until successive states converge. The model has been used by Izmodenov et al. (1999) to try to infer the local interstellar electron density from the passage of interstellar H through the heliospheric boundaries.

However, as discussed below, a time-dependent model of the heliosphere develops physical (not numerical) instabilities similar to a Rayleigh-Taylor instability at the nose of the HP and analogous to a Kelvin-Helmholtz instability on the flanks (Zank et al. 1996d; Liewer et al. 1996; Wang and Belcher 1998; Zank 1999d; Florinski et al. 2005a, Borovikov et al. 2008a, 2008b), these being driven by the "frictional" coupling of neutrals to plasma in the vicinity of a contact or tangential discontinuity. We therefore need to treat the steady-state heliospheric structure problem as time-dependent, with a time-scale of the order of the instability growth time. To improve statistics, and since the physical problem is devoid of time-scales, we can run the Monte-Carlo code for longer times, while running the plasma code for a much shorter time (of the order of a few years) to suppress the instability.

The Boltzmann code developed independently by Heerikhuisen et al. (2006, 2006b, 2008b) traces a large number of macro-particles on their orbit through the heliosphere. The H atoms move ballistically for a distance of the order of their (local) mean free path, before charge-exchanging with a proton picked at random from the local plasma. At this point

the process repeats with the new H atom inheriting the momentum of its parent proton. A splitting procedure is utilized to improve source term statistics in regions of large plasma gradients.

The loss term (2) may be simplified somewhat since both the Baranov & Malama and the original Heerikuisen et al. formulations assumed a Maxwellian distribution for the protons. In this case we can use the expressions developed in Ripken and Fahr (1983) and Pauls et al. (1995). Heerikhuisen et al. (2008a, 2008b) have extended their original formulation to draw particles from a κ distribution rather than a Maxwellian, and this is discussed further below.

During a charge-exchange event, a proton partner must be drawn from the plasma distribution. In the case of a Maxwellian plasma distribution, the probability distribution for the velocity of this partner will not simply be a Maxwellian, due to a selection effect caused by the distribution of individual particle velocities. Using a 3D analog of the 2D procedure described in Lipatov et al. (1998) yields the charge exchange frequency as a function of proton velocity of the form

$$\nu \propto |\mathbf{v}_H - \mathbf{v}_p|^2 \exp\left[-\frac{(\mathbf{v}_p - \mathbf{u}_p)^2}{v_{th,p}^2}\right], \tag{15}$$

where $\mathbf{v}_H$ and $\mathbf{v}_p$ are the atom and ion velocities and $\mathbf{u}_p$ is the bulk averaged plasma velocity (see also Malama 1991). Physically, this result confirms the intuitive notion that fast neutrals encounter charge-exchange partners more frequently.

As discussed above, the heliosphere–LISM environment can be described as either three or four thermodynamically distinct regions; the supersonic solar wind (region 3), the very hot subsonic solar wind (region 2), and the LISM itself (region 1a and 1b). Each region acts as a source of neutral H atoms whose distribution reflects that of the plasma distribution in the region. Accordingly, Zank et al. (1996d) identified neutral components 1, 2, and 3 with neutral atoms originating from regions 1, 2, and 3. Each of these three neutral components is represented by a distinct Maxwellian distribution function appropriate to the characteristics of the source distribution in the multi-fluid models. This observation allows the simplification of the production and loss terms (2) and (3) for each neutral component. The complete highly non-Maxwellian H distribution function is then the sum over the three components, i.e.,

$$f(\mathbf{x}, \mathbf{v}, t) = \sum_{i=1}^{3} f_i(\mathbf{x}, \mathbf{v}, t), \tag{16}$$

and for each component, the integral equation (1) must, in principle, be solved. Instead of solving (1), Zank et al. (1996d) use (16) in (1) to obtain three Boltzmann equations corresponding to each neutral component. This is an extension of the procedure developed in Pauls et al. (1995). For component 1, both losses and gains in the interstellar medium need to be included, but only losses are needed in the heliosheath and solar wind. This applies similarly to components 2 and 3. Thus, for each of the neutral H components i ($i = 1, 2$ or 3)

$$\frac{\partial f_i}{\partial t} + \mathbf{v} \cdot \nabla f_i = \begin{cases} P_1 + P_2 + P_3 - \beta_{ex} f_i & \text{region } i \\ -\beta_{ex} f_i & \text{otherwise} \end{cases}, \tag{17}$$

where $P_{1,2,3}$ means that P_{ex} is to be evaluated for the parameters of components 1, 2, or 3 respectively. Under the assumption that each of the neutral component distributions is approximated adequately by a Maxwellian, one obtains immediately from (17) an isotropic

hydrodynamic description for each neutral component,

$$\frac{\partial \rho_i}{\partial t} + \nabla \cdot (\rho_i \mathbf{u}_i) = Q_{\rho i}; \tag{18}$$

$$\frac{\partial}{\partial t}(\rho_i \mathbf{u}_i) + \nabla \cdot \left[\rho_i \mathbf{u}_i \mathbf{u}_i + p_i \mathbf{I}\right] = \mathbf{Q}_{mi}; \tag{19}$$

$$\frac{\partial}{\partial t}\left(\frac{1}{2}\rho_i u_i^2 + \frac{p_i}{\gamma - 1}\right) + \nabla \cdot \left[\frac{1}{2}\rho_i u_i^2 \mathbf{u}_i + \frac{\gamma}{\gamma - 1}\mathbf{u}_i p_i\right] = Q_{ei}. \tag{20}$$

The source terms Q are appropriate moments of (2) and (4) and are listed in Pauls et al. (1995) and Zank et al. (1996d). The subscript i above refers to the neutral component of interest ($i = 1, 2, 3$), ρ_i, $\mathbf{u}_i$, and p_i denote the neutral component i density, velocity, and isotropic pressure respectively, $\mathbf{I}$ the unit tensor and γ ($= 5/3$) the adiabatic index.

Heerikhuisen et al. (2006) explore the similarities and differences between multi-fluid and Monte-Carlo models of the heliosphere and compare their Monte-Carlo code (similar in many respects to that developed by Malama 1991) with a four-neutral fluid code, which is a straightforward extension of the original 3-fluid neutral code of Zank et al. (1996d) that subdivides region 1 into regions 1a and 1b. They also compare their models to those of Alexashov and Izmodenov (2005), using the same parameters and boundary conditions for a variety of fluid and kinetic models. For this comparison, Heerikhuisen et al. (2006) used relatively simple axially symmetric models without magnetic fields and considered only steady-state solutions. Surprisingly good comparative results were found between kinetic and multi-fluid models, especially in global features, structure, and location, and between the UAH and Moscow groups models. While the axially symmetric models have now been superseded by more sophisticated 3D models, they nonetheless allow one to probe much of the basic physics of the solar wind-LISM interaction simply and efficiently, and in particular, allow for more accurate kinetic modeling since the neutral H statistics can be done very accurately. Pogorelov et al. (2008a, 2008) have extended the comparison of multi-fluid and kinetic approaches to 3D, and some of these results are discussed below.

3 Role of Magnetic Fields and Neutral H in Determining Heliospheric Structure

Both the interplanetary and interstellar magnetic field affect the shape and position of the HP relative to the Sun and interstellar plasma velocity vector, originally discussed by Fahr et al. (1988), Linde et al. (1998), Pogorelov and Semenov (1997), Pogorelov and Matsuda (2000), and Ratkiewicz et al. (1998). The interplanetary magnetic field (IMF), by virtue of the current sheet, introduces a corresponding asymmetry inside the inner heliosheath that also affects the shape and position of the HP (Washimi and Tanaka 1996, 2001; Linde et al. 1998; Zank 1999). The asymmetry in the HP position affects the shape of the heliospheric TS, and the different distances at which the V1 and V2 TS crossings occurred suggests that some asymmetry in the TS position exists (Stone et al. 2008). Prior to the V1 and V2 crossings of the TS, Lallement et al. (2005) suggested that an asymmetry in the plasma distribution on the interstellar side of the HP might be responsible for the deviation of the H-atom and He-atom flows observed in the inner heliosphere by the SOHO SWAN experiment.

In an effort to more carefully identify the role of the ISMF in introducing an asymmetric heliospheric structure, Pogorelov et al. (2004) reconsidered the ISMF coupling with the IMF at the HP using an ideal MHD plasma model in the absence of neutral H.

A range of different orientations of the ISMF $\mathbf{B}_\infty$ with respect to the interstellar flow vector $\mathbf{V}_\infty$ and the ecliptic plane was considered to determine the resulting TS and HP location and shape. Like other related studies (Ratkiewicz et al. 1998; Opher et al. 2006; Washimi et al. 2006), the ISMF can have a significant effect on the global structure and symmetry of the TS and HP. However, all these studies neglect the self-consistent inclusion of neutral H, which acts to symmetrize the heliosphere, therefore reducing the asymmetric effects of the ISMF (Pogorelov et al. 2006; Pogorelov and Zank 2006; Pogorelov et al. 2007). Global models of the heliosphere that properly include neutral H have relatively small hemispheric asymmetries compared to models that neglect neutrals, and if larger asymmetries are observed, then the likely cause is probably the result of a highly temporal solar wind (Zank and Müller 2003; Washimi et al. 2007b).

The SOHO SWAN experiment observations by Lallement et al. (2005) showing a $4° \pm 1°$ deflection of the H-atom flow from the interstellar He-atom flows in the inner heliosphere offers an interesting possible opportunity to extract some information about the strength and orientation of the ISMF. Izmodenov et al. (2005), estimated the direction of the H-atom flow in the inner heliosphere by analyzing statistically averaged trajectories of neutral H atoms for a model that neglected the IMF and assumed a spherically-symmetric solar wind. Not surprisingly, this ensured that the heliosphere was symmetric with respect to the plane formed by $\mathbf{B}_\infty$ and $\mathbf{V}_\infty$ (a BV-plane). Consequently, an average neutral H trajectory which starts at a LISM point in the BV-plane will remain in that plane. By contrast, those trajectories that start at two points lying symmetrically above and below the BV-plane will acquire out-of-plane velocity components oriented in the opposite directions, making the average out-of-plane deflection zero. A better and more careful analysis by Pogorelov et al. (2006) and Pogorelov and Zank (2006) showed that the flow of neutral H never preserves its original unperturbed LISM orientation, even for $\mathbf{B}_\infty \parallel \mathbf{V}_\infty$. Moreover, for models that include the IMF, the H deflection inevitably takes place both within and perpendicular to the BV-plane. Thus, the H deflection plane (HDP) and the BV-plane do not typically coincide.

It does not necessarily follow that the observed $4° \pm 1°$ deflection of H-atoms from its LISM vector implies a highly obliquely oriented ISMF. The deflection of H parallel and perpendicular to the BV-plane can be comparable if the angle between $\mathbf{B}_\infty$ and $\mathbf{V}_\infty$ is not large (Pogorelov and Zank 2006). However, to produce a $4° \pm 1°$ deflection requires a strong ISMF (perhaps greater than 5 μG) for $\mathbf{B}_\infty$ lying at small angles to $\mathbf{V}_\infty$. Although not commonly assumed as ISMF values, such strengths should not be disregarded. The Cox and Helenius (2003) theory for the origin of the Local Bubble suggests a strong ISMF lying nearly parallel to the LISM velocity vector. Obviously, since magnetic pressure acts perpendicularly to magnetic field lines, an increase in $\mathbf{B}_\infty$ will not unduly affect the TS and HP stand-off distances in the upstream LISM directions (Baranov et al. 1971; Florinski et al. 2004a). However, increasing $\mathbf{B}_\infty$ may well yield a LISM flow speed that is either sub-fast magnetosonic or even sub-Alfvénic. Even for this case, Florinski et al. (2004a) (2D) and Pogorelov et al. (2006) (3D) found global heliospheric solutions that had the HP at a finite distance from the Sun, provided interstellar neutral H was included self-consistently.

To include the self-consistent coupling of neutral H atoms and a magnetized plasma, Pogorelov et al. (2006) extended the two-fluid and four-fluid models of Pauls et al. (1995) and Zank et al. (1996b) to include magnetic fields in a full MHD description. As already discussed, this is a reasonable approximation whenever we are interested primarily in the role of the magnetic field. The 4-fluid interaction model has proved effective in modeling 3D (Pauls and Zank 1997b), magnetized but axi-symmetric (Florinski et al. 2003a), and non-stationary aspects of the solar wind-LISM interaction (Zank 1999a; Zank and Müller 2003). The review by Zank et al. (2008) compares purely MHD models and models that include

neutral H self-consistently for a variety of ISMF $\mathbf{B}_\infty$ orientations relative to the interstellar flow vector $\mathbf{V}_\infty$. We may anticipate, on the basis of numerous gas dynamical calculations, that the influence of charge exchange on global heliospheric structure is likely to be stronger than the effect of a weak ISMF.

The numerical calculations are based on a Cartesian coordinate system with origin at the Sun. The x-axis is oriented along the Sun's rotation axis, perpendicular to the ecliptic plane (yz-plane), for simplicity. The z-axis belongs to the plane defined by the x-axis and $\mathbf{V}_\infty$, and is directed toward the LISM. The y-axis completes the coordinate system.

Here we consider two cases, the first being $\mathbf{B}_\infty \perp \mathbf{V}_\infty$, and the other with $\mathbf{B}_\infty$ in the HDP.

Consider the case of $\mathbf{B}_\infty \perp \mathbf{V}_\infty$ and $\mathbf{B}_\infty \perp 0x$ modeled using a two-fluid approach. Figure 3 shows the plasma density (Fig. 3a; logarithmic scale), magnetic field strength (Fig. 3b), plasma temperature (Fig. 3c; logarithmic scale), and neutral H density (Fig. 3d) distributions. The structure of the heliosphere when neutral H is included self-consistently is substantially different from that derived from a purely MHD model. The distance to the TS is decreased considerably and the bullet-shape, so characteristic of models (both gas dynamic and MHD) that exclude the neutral H, is absent. Both effects are of course due to the deceleration of supersonic flows by the pickup process.

From the plot of the magnetic field strength (Fig. 3b), it is seen that the heliospheric current sheet (HCS), assumed to lie in the ecliptic instead of being tilted, bends into the lower hemisphere. As a result, some IMF lines from the upper hemisphere are carried by the solar wind to the lower hemisphere. The IMF and ISMF vectors at the upwind section of the HP are oriented approximately in the same direction. Further downstream, the HCS width increases, it interacts with the (numerically diffusive) HP, and we observe ripples on its surface. Since the IMF and ISMF are oppositely directed in the lower hemisphere, the ripples most likely result from a combination of numerical magnetic reconnection between the IMF and ISMF lines (see Pogorelov et al. 2004) and possibly a Kelvin-Helmholtz-type instability of the HP, perhaps driven by neutral H (Borovikov et al. 2008b; Zank 1999d; Florinski et al. 2003b). In particular, the temperature of the LISM protons increases due to the energy released by reconnection. The HP is asymmetric with respect to the ecliptic plane, and it also appears that the maximum IMF magnitude on the inner side of the HP is about 10% greater in the upper hemisphere than in the lower, and the region of the enhanced IMF is more extended there.

The other $\mathbf{B}_\infty \perp \mathbf{V}_\infty$ example that we discus is that of $\mathbf{B}_\infty$ tilted 60° to the ecliptic plane. Figure 4 shows the distributions of the plasma density (Fig. 4a), the magnetic field strength (Fig. 4b), the plasma density (Fig. 4c), and the population 1 neutral H (Fig. 4d) in the meridional plane for the four-fluid model. Comparing two-fluid and four-fluid models (Zank et al. 1996b; Pogorelov et al. 2006) shows that the bow shock standoff distance from the HP is larger in the four-fluid approximation, while the maximum values of the plasma density and magnetic field are noticeably smaller. The width of the hydrogen wall is greater, while the increase in the neutral H density is smaller. The distribution of the IMF strength is qualitatively similar for both four- and two-fluid models. Worth noting is an essentially 3D effect showing an asymmetry in the population 2 hydrogen distribution with respect to the ecliptic plane. A more detailed analysis of the distribution of quantities in the upwind direction is presented in Figs. 9–11 of Pogorelov et al. (2006). They find that the bow shock, HP, and TS distances to the Sun obtained with the four-fluid model are somewhat larger than those calculated with the two-fluid model, with the differences consecutively decreasing (295, 137, and 95 AU and 329, 152, and 102 AU for the two- and four-fluid models, respectively). The TS distances to the Sun in the downwind direction are about 211 AU for both models. This result differs significantly from that presented in the paper of Alexashov and Izmodenov (2005), where a two-fluid model (a one-fluid neutral model in their terminology) gave

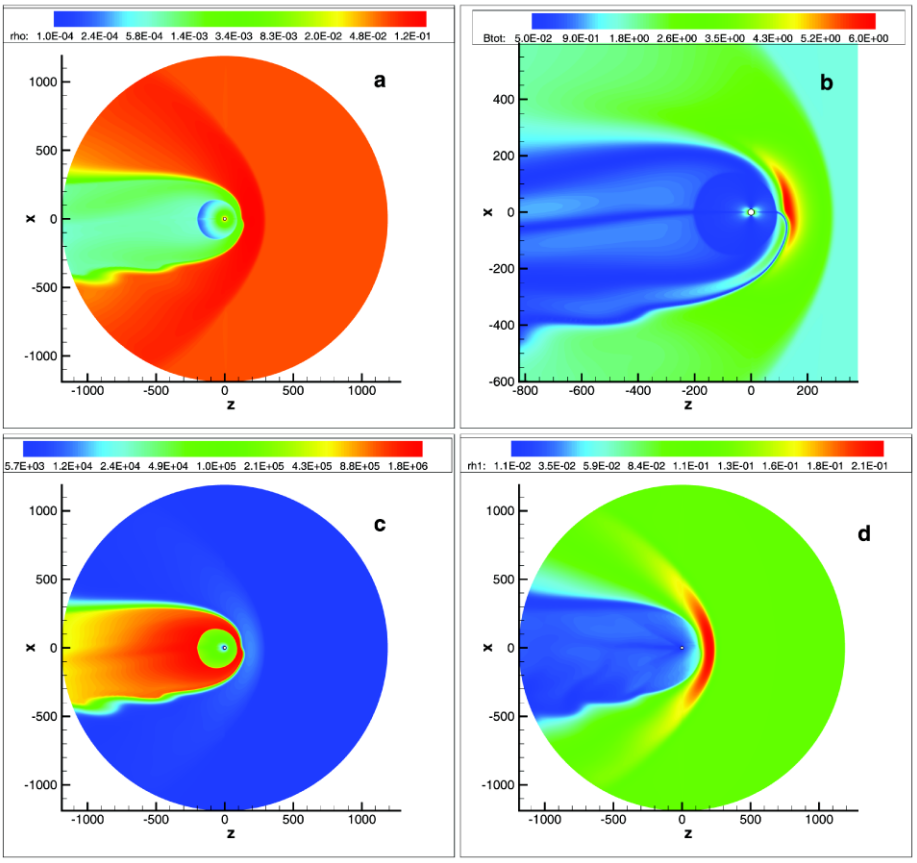

Fig. 3 Distributions in the meridional plane for the solar wind–LISM interaction the case of $\mathbf{B}_\infty \perp \mathbf{V}_\infty$ and $\mathbf{B}_\infty \perp 0x$ in the two-fluid model approximation: (**a**) plasma density (logarithmic scale) in particles per cm^{-3}, (**b**) magnetic field strength in μG, (**c**) plasma temperature (logarithmic scale) in K, and (**d**) neutral H density in particles per cm^{-3}. $B_\infty = 1.5$ μG. The distance along both axes is measured in AU, centered on the Sun (the origin). (Pogorelov et al. 2006)

a difference in the TS downwind locations greater than 50% of that in the kinetic model. A possible reason might be their somewhat different treatment of the secondary hydrogen atoms. Although both models take into account momentum loading of the solar wind plasma properly, Alexashov and Izmodenov (2005) neglect only the secondary hydrogen atoms that originate in the supersonic solar wind, whereas our model neglects them everywhere in the solar wind and heliosheath. This may be a possible reason why the one-, two-, and three-fluid hydrogen models of Alexashov and Izmodenov (2005) give results so different from those in the four-fluid model. The discrepancy is smaller if our approach is applied. On the other hand, discrepancies between different multi-fluid models may potentially increase with increasing number density of interstellar H atoms.

Figure 5 shows the distributions of the magnetic field magnitude B_{tot} (solid lines) and the Cartesian components B_x (dashed lines), B_y (dot-dashed lines), and B_z (double-dot-dashed lines) of the magnetic field vector in the meridional plane for lines of sight slightly above (left) and slightly below the ecliptic plane (right). Thicker lines correspond to a two-fluid

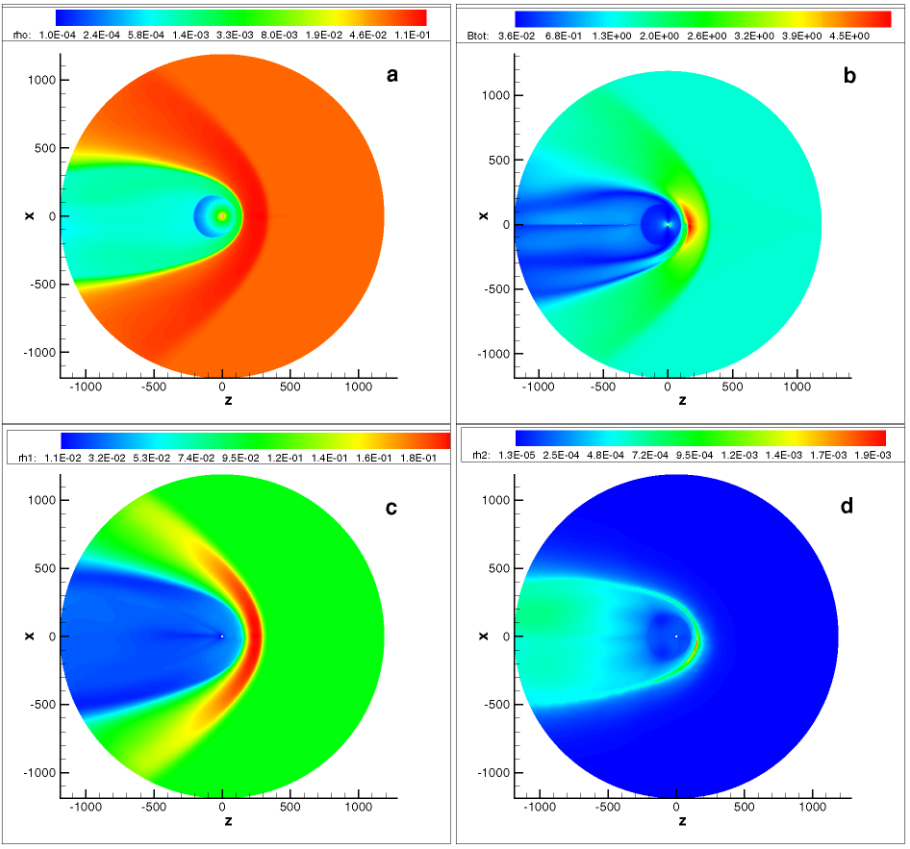

Fig. 4 Distributions in the meridional plane for the solar wind–LISM interaction for the case of $\mathbf{B}_\infty \perp \mathbf{V}_\infty$ and tilted 60° to the solar ecliptic plane in the four-fluid model approximation: (**a**) plasma density (logarithmic scale) in particles per cm^{-3}, (**b**) magnetic field strength in μG, (**c**) plasma temperature (logarithmic scale) in K, and (**d**) neutral H density in particles per cm^{-3}. $B_\infty = 1.5$ μG. The distance along both axes is measured in AU, centered on the Sun (the origin). (Pogorelov et al. 2006)

model. A decrease in the magnetic field strength occurs when the line of sight intersects the HCS. The distribution of the magnetic field is asymmetric with respect to the ecliptic plane, which may well lead to related asymmetries in the cosmic-ray modulation in opposite hemispheres.

On the basis of a kinematic magnetic field model, Zank (1999) suggested the possibility that the IMF may cross the TS multiple times. Jokipii and Giacalone (2004), Jokipii et al. (2004), and Stone et al. (2005) have suggested this as an explanation for the V1 observations of several month-long increases in energetic particle fluxes in late 2002–2003. Since the shape of the TS does not coincide with the shape of the Parker spiral magnetic field in the upwind region, it is therefore possible (Zank 1999; McDonald et al. 2003) that some IMF lines can reappear in the upstream solar wind region after crossing the TS from the downstream side. This possibility was analyzed carefully by Pogorelov et al. (2006) using their self-consistent 3D IMF distribution, finding that this is indeed the case. It was shown that the self-consistent inclusion of neutral H ensures that V2 could not be directly connected

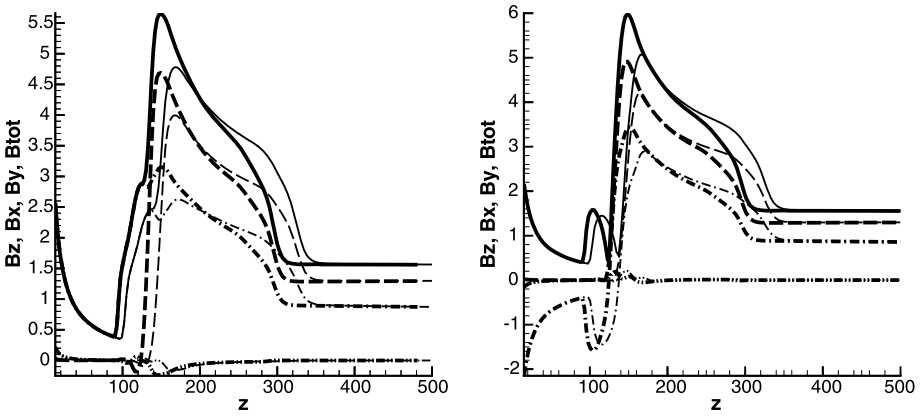

Fig. 5 (*Left*) Distributions of the magnetic field magnitude (*solid lines*), B_x (*dotted lines*), B_y (*dot-dashed lines*), and B_z (*double-dot-dashed lines*) components of the magnetic field vector in the meridional plane along a line of sight slightly above the ecliptic plane (in μG as a function of AU). (*Right*) Corresponding distributions in the meridional plane along a line of sight slightly below the ecliptic plane. The two-fluid results are shown by *thick lines*. (Pogorelov et al. 2006)

magnetically to the TS if the radial separation between V2 and the TS was greater than 3 AU, even for $\mathbf{B}_\infty$ as large as 3 μG (Pogorelov et al. 2007).

A critical observational result was the measurement of the deflection of H atoms from the interstellar He trajectory by Lallement et al. (2005). Pogorelov et al. (2008c), building on earlier studies by Heerikhuisen et al. (2006, 2007) and Pogorelov et al. (2008a), used a fully time-dependent 3D MHD-kinetic model to consider the effect of $\mathbf{B}_\infty$ lying in the HDP. This code incorporates both solar wind and LISM magnetic fields, and couples an MHD code self-consistently to a time-dependent 3D Monte-Carlo code that determines the kinetic distribution of neutral H. The LISM plasma velocity, temperature and density for their simulations are assumed to be $\mathbf{B}_\infty = 26.4\ \mathrm{km\,s^{-1}}$, $T_\infty = 6527$ K, and $n_\infty = 0.06\ \mathrm{cm^{-3}}$, respectively, and the density of neutral H is $n_{H\infty} = 0.15\ \mathrm{cm^{-3}}$. The solar wind is assumed to be spherically symmetric with the following parameters at 1 AU: $V_E = 450\ \mathrm{km\,s^{-1}}$, $T_E = 51,100$ K, and $n_E = 7.4\ \mathrm{cm^{-3}}$. The magnitude of the ISMF vector is $\mathbf{B}_\infty = 3$ μG. The radial component of the IMF at 1 AU is set to 37.5 μG, and we assume a Parker spiral at 1 AU. For convenience and to allow for easy visualization of the various planes and symmetries, we plot the coordinate system in Fig. 6. The direction of the LISM velocity is aligned with the vector $\mathbf{l}_{\mathrm{He}} = (-0.087156, 0, -0.9962)$. The HDP is defined by $\mathbf{l}_{\mathrm{He}}$ and the vector $\mathbf{l}_{\mathrm{H}} = (-0.1511, -0.04049, -0.9877)$ corresponding to the direction that LISM neutral H enters the inner heliosheath determined observationally by Lallement et al. (2005). We assume that $\mathbf{B}_\infty$ is aligned with the vector $\mathbf{l}_B = (-0.5, -0.2678, -0.82356)$. Thus, $\mathbf{B}_\infty$ belongs to the observed HDP and is directed into the southern hemisphere at an angle of $\sim 30°$ to the ecliptic plane. This direction gave one of the largest V1–V2 asymmetries of the TS in the two-fluid calculations of Pogorelov et al. (2007). In fact, $\mathbf{B}_\infty$ in the plane tilted at 60° to the ecliptic plane is very close to the observed HDP (Pogorelov et al. 2007, 2006).

Figure 7 shows the distribution of the plasma temperature in the V1–V2 plane, illustrating that, in agreement with the two-fluid calculations of Pogorelov et al. (2007), the asymmetry of the TS is minor. Both two-fluid and multi-fluid models show that the asymmetry of the TS is rather small, unlike the ideal MHD calculations of Opher et al. (2006) where the absence of neutral H exaggerates the asymmetry. In Fig. 8, we show the distributions of the proton

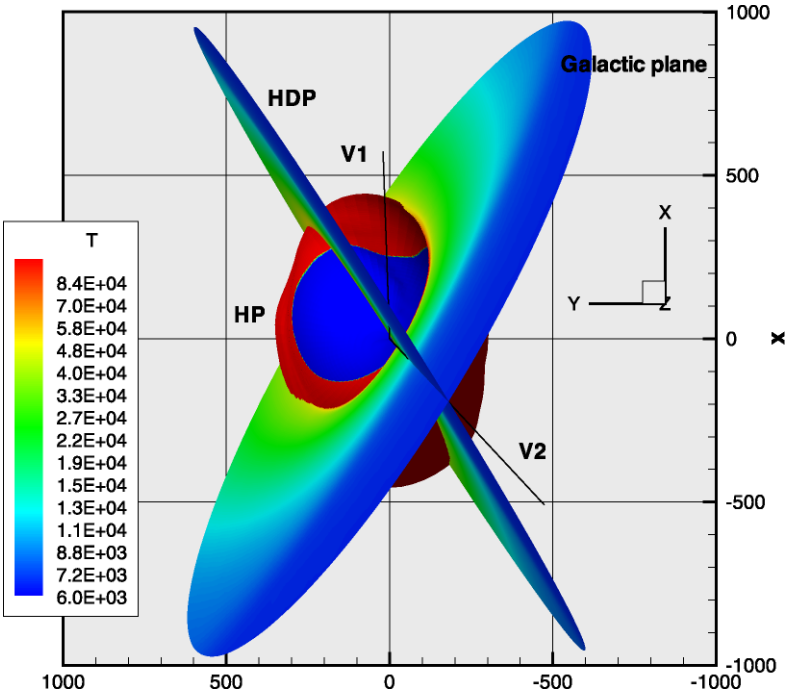

Fig. 6 Frontal view of the HP, HDP, Galactic plane, and V1 and V2 trajectories. *Blue* and *red colors* on the surface of the HP correspond to $B_R < 0$ and $B_R > 0$, respectively. The planes are colored according to the plasma temperature (K) distributions. The HP is clearly asymmetric with respect to the BV-plane. The axes are in AU, measured from the Sun (the origin). (Pogorelov et al. 2008b)

temperature along sight lines in the direction of V1 (solid black lines) and V2 (solid red lines). For the sake of comparison, Pogorelov et al. (2006) also use dashed lines to show the same distributions obtained with a five-fluid model.[1] In Fig. 9, we compare radial profiles of the plasma density and magnetic field magnitudes obtained using a five-fluid and MHD-kinetic model respectively (Pogorelov et al. 2008a, 2008). The colored lines correspond to the directions $\phi = 180°$, $\theta = 35°$ (black), $\phi = 0°$, $\theta = 0°$ (red), $\phi = 0°$, $\theta = 90°$ (green), and $\phi = 0°$, $\phi = 180°$ (purple). The angles ϕ and θ are measured from the x-axis in the xy-plane and from the z-axis, respectively. Clearly, the results obtained from these two different models are in a excellent qualitative and even quantitative agreement.

An interesting result to emerge from this simulation is that the kinetic treatment of charge exchange leads to the disappearance of the bow shock, which is essential in an equivalent ideal MHD model. The disappearance of the bow shock is a direct consequence of the secondary charge exchange of hot neutral H created in the inner heliosheath in the LISM. Hot neutral H created in the inner heliosheath has high thermal velocities, so these particles move easily into the LISM upstream of the bow shock. The subsequent secondary charge

[1]The five-fluid model extends the original multi-fluid model of Zank et al. (1996d) by using the ideal MHD equations to model the flow of protons and four (instead of three) coupled sets of Euler equations to simulate the flow of separate neutral H fluids. These consist of the parent LISM neutrals (population 1a) and those born in the outer heliosheath (population 1b), inner heliosheath (population 2), and supersonic solar wind (population 3).

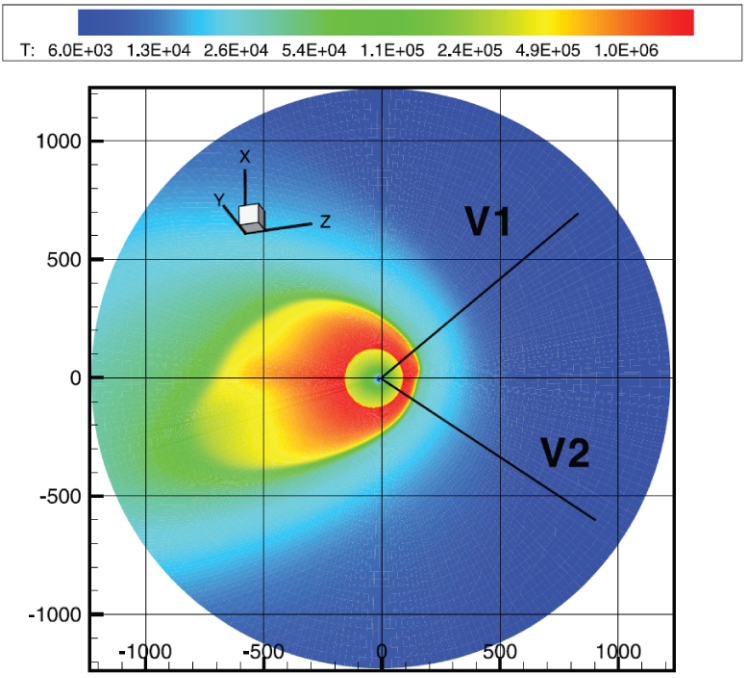

Fig. 7 Plasma temperature (K) distribution in the V1–V2 plane. The *straight lines* show the V1 and V2 trajectories and the axes are plotted in AU. (Pogorelov et al. 2008a)

exchange leads to anomalous heating of the LISM plasma ahead of the HP and the bow shock, which increases the sound speed and thus reduces the interstellar flow Mach number (to the point that the flow becomes subsonic!).

The symmetrizing effect of charge exchange in the presence of an ISMF is easily understood. For the chosen solar wind and LISM parameters, neglecting the neutral particles results in the HP rotating so that the nose is shifted to the south while the tail is shifted to the north (Pogorelov et al. 2007). As a result, the stagnation point of the LISM plasma on the HP moves above the ecliptic plane. This creates an asymmetric distribution of the LISM plasma in the outer heliosheath, which results in enhanced charge exchange in this region. Charge exchange created pickup ions exert additional pressure, which acts to decrease the asymmetry of the HP by counterbalancing the ISMF pressure. A similar mechanism works on the solar wind side of the HP. Pogorelov et al. (2008a) find that the TS is closer to the Sun by only about 3 AU in the V2 direction than the V1 direction in their MHD-kinetic simulation—see Fig. 8. The steady-state asymmetry is far too small to explain a V2 crossing of the TS at a distance to the Sun closer by 10 AU than V1. Instead, it is likely that temporal variations in the solar wind ram pressure modify the TS location significantly (Scherer and Fahr 2003; Zank and Müller 2003; Borrmann and Fichtner 2005; Pogorelov et al. 2007; Washimi et al. 2007a, 2007b), offsetting the effect of the ISMF pressure.

The MHD-neutral analysis of Pogorelov et al. (2007) shows that east-west asymmetry of the TS due to the ISMF in the observed HDP is also insufficiently large to allow V2 to be directly (by less than a full winding of the IMF spiral) connected to the TS at distances larger than about 3 AU ahead of the TS. Energetic protons with energies less than 7 MeV cannot stream along a field line from the TS to V2 directly.

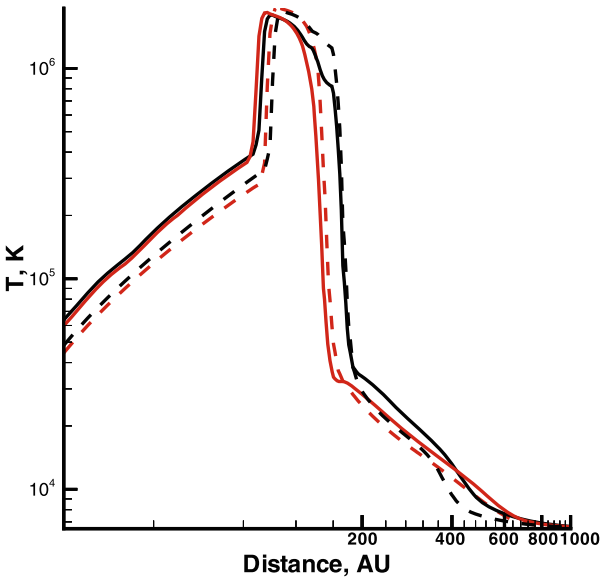

Fig. 8 Distribution of plasma temperature (K) in the V1 (*black lines*) and V2 (*red lines*) directions. The results shown with *solid* and *dashed lines* were obtained using an MHD-kinetic and a five-fluid model respectively. (Pogorelov et al. 2008a)

Experience shows that a larger component of $\mathbf{B}_\infty$ parallel to the ecliptic plane increases the TS asymmetry. This may result, however, in an H flow deflection greater than that observed in the SOHO SWAN experiment since the two effects are mutually related. To quantify the effect of the neutral H flow deflection, Pogorelov et al. (2008a) used their kinetic neutral-atom code to collect statistics on the H-atom velocity distribution in the solar wind. They recorded the deflection from $\mathbf{V}_\infty$ of all H-atoms within a 45° cone about $\mathbf{V}_\infty$ out to 80 AU, both in the BV-plane and perpendicular to it, thus creating a two dimensional distribution of deflections. In Fig. 10, we show the primary (population 1a) LISM H-atoms (left panel), secondary (population 1b) H-atoms (middle panel), and the total (weighted) distribution (right panel) in the plane perpendicular to $\mathbf{V}_\infty$. Although the primary LISM distribution is initially Maxwellian, its interaction with the heliosphere results in a distribution of deflections that is obviously not isotropic. This is because charge-exchange losses preferentially cull a particular part of the distribution due to asymmetric plasma flow and the dependence of the charge-exchange rate on the relative plasma flow speed. Secondary H-atoms, and thus the combined distribution, are clearly not isotropic, and the mean of the distribution does not coincide with its center, making it more difficult to quantify the overall deflection. We find that the average deflection of primary neutrals is about 1.8° in the BV-plane and −0.18° perpendicular to this plane. For secondary neutrals, the corresponding values are 4.7° and 0.15°, and for the combined population these are 3.8° and 0.05°. The peaks of the distributions are not at these locations; and instead, the primary population shows a peak close to zero deflection, and the most common deflection of the secondary neutrals is around 7° in the BV-plane and 1° out of it. For this particular example, the average deflection takes place almost entirely in the BV-plane. Thus, the actual angle between the BV-plane and the HDP is determined by the accuracy in measuring the H-flow direction by the SOHO SWAN experiment, which is to within 1°. Although Pogorelov et al. (2008a) assume that the BV-plane is parallel to the average HDP, an additional deflection of the order of ±1° perpendicular to the average HDP cannot be excluded. This gives us an estimate for the angle between the HDP and BV-plane as $\arctan(\tan 1^\circ / \tan 4^\circ) = 15^\circ$ (Pogorelov et al. 2007).

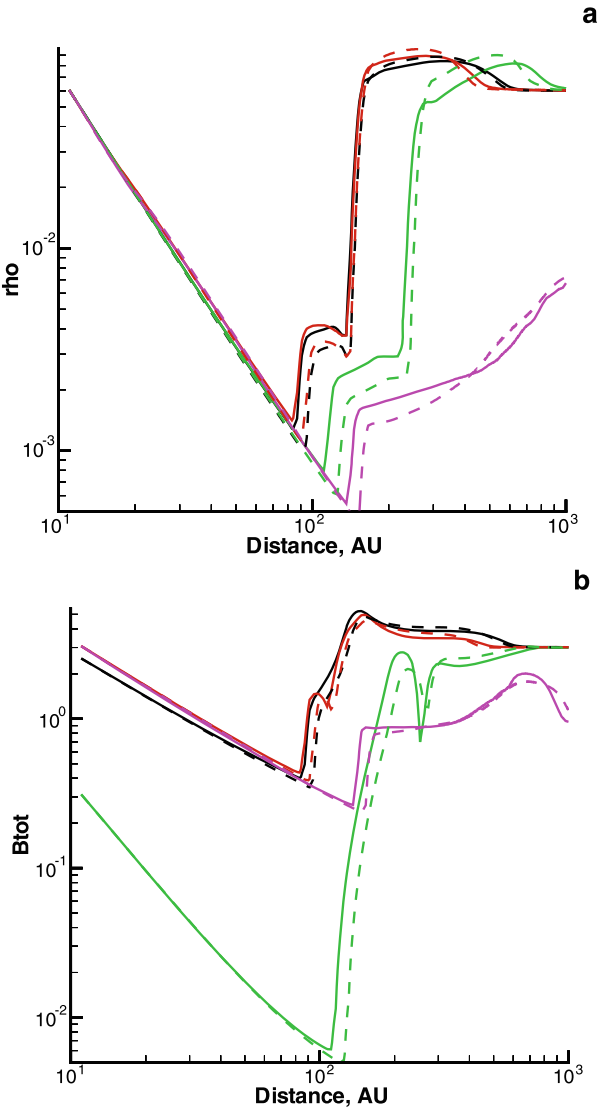

Fig. 9 Distribution of (**a**) plasma number density (in cm^{-3}) and (**b**) magnetic field magnitude (in μG) along the directions $\phi = 180°$, $\theta = 35°$ (*black lines*), $\phi = 0°$, $\theta = 0°$ (*red lines*), $\phi = 0°$, $\theta = 90°$ (*green lines*), and $\phi = 0°$, $\phi = 180°$ (*purple lines*). The results shown with *solid* and *dashed lines* correspond to an MHD-kinetic and a five-fluid model, respectively. (Pogorelov et al. 2008)

The effect of a stronger IMF was discussed by Pogorelov et al. (2008c), who found that $B_\infty \sim 7$ μG can increase the TS asymmetry to 8 AU.

In summary, MHD-only models that neglect the self-consistent inclusion of neutrals at either a multi-fluid or kinetic level cannot adequately describe global heliospheric structure, and the ideal MHD models of Pogorelov et al. (2004) and Opher et al. (2006) are inappropriate in this context. The Opher et al. model, to arrive at some quantitative results, uniformly scales the ideal MHD solution to the known distance of the TS crossing by V1, but as we have shown explicitly above for both gas dynamic and MHD models, the TS heliocentric distance can be 1.5 times larger when neutral particles are neglected, even for identical SW and LISM conditions (Zank 1999).

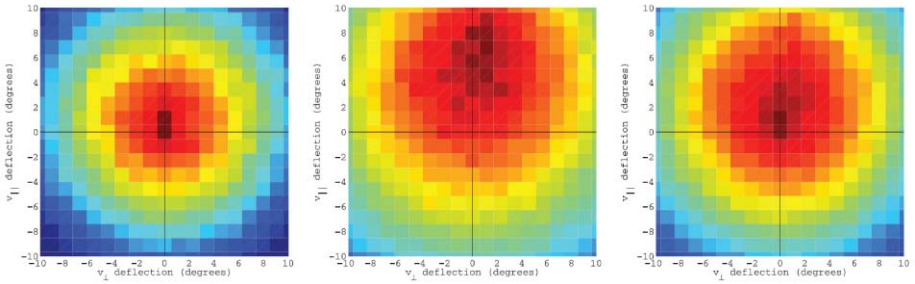

Fig. 10 Two-dimensional distribution of H-atom deflections (measured in degrees) from $\mathbf{V}_\infty$ in the plane perpendicular to the LISM BV-plane (the interstellar perspective), showing (*left*) primary interstellar H-atoms, (*middle*) secondary H atoms (i.e., the last charge-exchange occurred in the outer heliosheath), and (*right*) the combined distribution. The normal is determined by the vector product $\mathbf{r}_H \times \mathbf{r}_{He}$. The *darkest red color* corresponds to a particle count twice larger than that of the *darkest blue color*. (Pogorelov et al. 2008)

4 Termination Shock (TS) Response to Interplanetary Disturbances

Recent 3D MHD simulations by Washimi et al. (2007a, 2007b) confirmed that solar-wind ram-pressure variability contributed to the variability in R_{TS}, the distance of the TS from the Sun. The heliopause too responds to supersonic solar wind disturbances, although with a delay corresponding to the transit-time of transmitted disturbances in the heliosheath (Karmesin et al. 1995; Zank and Müller 2003). The variability of the solar wind therefore plays an important role in the global heliospheric dynamics. Washimi et al. (2007b) discuss the response of R_{TS} to solar wind ram-pressure changes. They initially consider a stationary heliosphere assuming fixed inner (solar wind) and outer boundary (ISM) conditions, and then analyze the heliosheath response by generating simplified solar-wind ram-pressure pulses in the supersonic solar wind. This simplified simulation reveals the considerable effect on R_{TS} by large amplitude incident, transmitted, and reflected heliosheath disturbances. A realistic and time-varying inner boundary using V2 plasma data is then incorporated in their 3D MHD simulation, which yields a temporal R_{TS}. By using the most current V2 data, Washimi et al. (2007b) somewhat boldly attempted to forecast the future TS position after making some reasonable assumptions about the overall solar wind ram-pressure for the next year. In part, a plausible forecast can be made because of the long transit time and response time of the global heliosphere to short timescale supersonic solar wind disturbances. The Washimi et al. (2007b) model did not include neutral H self-consistently but this is now done in a multi-fluid framework in their most recent (but unpublished) models.

Washimi et al. (2007a, 2007b) begin with a stationary global 3D MHD heliosphere. At the inner boundary of the initially stationary global 3D heliosphere, Washimi et al. (2007b) assign a set of standard values at 1 AU, i.e., density 5/cc, velocity 400 km/s (the ram-pressure of the standard set is $P_{ram,0} = 1.3 \times 10^9$ Pa at 1 AU), and toroidal magnetic field of 2.8 nT. The solar magnetic moment is assumed to be non-tilted, so that the toroidal magnetic field intensity on the inner boundary has a $\sin\theta$-dependence and its polarity reverses from northern to southern hemispheres, where θ is the colatitude measured from the solar-rotation axis z. The LISM flow speed relative to the Sun is 26.3 km/s along the x-axis, and proton density is 0.105/cc. As discussed already at length above, Washimi et al. assume that the ISMF is in the HDP (Lallement et al. 2005) has an intensity of 0.24 nT and components $\mathbf{B} = (0.163, -0.100, -0.145)$ nT. The LISM temperature is 10^4 K. Under these conditions, R_{TS} of the stationary heliosphere along the Sun–V1 line is $R_{TS,0} = 86$ AU. To obtain a reasonably realistic and time-varying heliosphere, Washimi et al. (2007a, 2007b) used

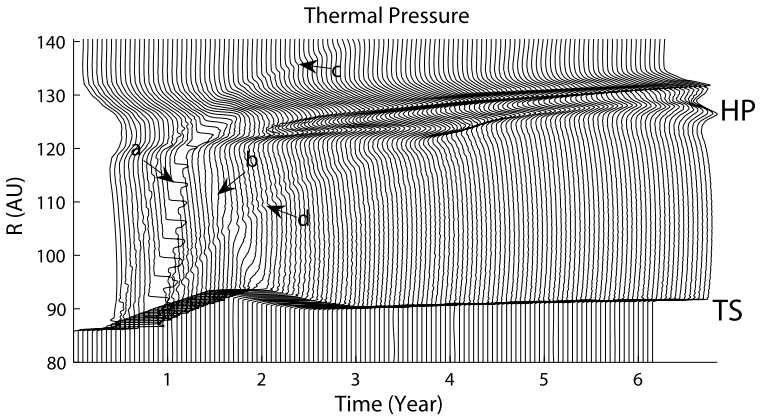

Fig. 11 Stacked space–time plots showing the propagation of the thermal pressure in the heliosheath and beyond when the solar wind ram-pressure steps increases abruptly from $P_{ram,0}$ to $1.5 \times P_{ram,0}$ at year 0. The *arrows* labeled (a), and (b), denote the forward and reflected thermal pressure pulses, and (c) and (d) the transmitted and convected pulses, respectively. The movement of the TS in response to both the incident and reflected pressure pulses is evident, as is the gradual relaxation of the TS to a new steady-state location because of the now higher (constant) solar wind ram pressure. (Washimi et al. 2007b)

V2 observed daily averaged solar wind velocity and density during the period 2001.9.10–2007.3.24 as their inner boundary condition. Under these conditions Washimi et al. (2007b) use an iterative method of simulation to determine a LISM density of 0.1107/cc that yields a V1-crossing at the observed time with an error of ≈ 10 days. Consequently, they adopt this parameter in their analysis. This of course does not correspond necessarily to a precise LISM number density but is a device to ensure that the TS location corresponds to the V1 data point, and is a method to mimic the presence of H atoms. Note that the magnetic field orientation is the same as used in Opher et al. (2006), whose plasma parameters result in a relatively large north–south (N–S) asymmetry. However, as already noted, the self-consistent inclusion of neutral H in the simulations strongly reduces the asymmetry, and Washimi et al. (2007b) are therefore extending their model to properly include interstellar atoms on the basis of a multi-fluid model (Zank et al. 1996d).

In this subsection, all analyzed quantities of the 3D Washimi et al. simulations are measured along the Sun–V1 or Sun–V2 line.

Starting from a stationary heliosphere, Washimi et al. (2007b) consider the response of the TS to discrete disturbances such as the solar wind ram-pressure changing step-wise from $P_{ram,0}$ to $1.5P_{ram,0}$. Figure 11 shows explicitly how and why the TS oscillates in location. A disturbance incident on shock must emit a series of waves and convected structures such that the shock satisfies the evolutionary conditions (e.g., McKenzie and Westphal 1968). For the case considered here, this is a fast mode wave and a convected entropy-vorticity wave. The emitted wave propagates to the HP at the magneto-acoustic speed $C_a \approx 524$ km/s, where it is partially reflected (the heliosheath is subsonic) and transmitted at the HP. The reflected wave propagates back to the TS at a speed $C_b \approx 210$ km/s. When the HP reflected pulse strikes the TS, the outward motion of the TS is reduced and R_{TS} begins to decrease. An increase in the magnetic pressure accompanies the thermal-pressure pulse. The reflected thermal-pressure pulse plays a surprisingly important role in determining the change of R_{TS}, being the reason that R_{TS} decreases continually for nearly a year even though the overall ram pressure of the solar wind increased. This effect is a consequence of both the propagation of

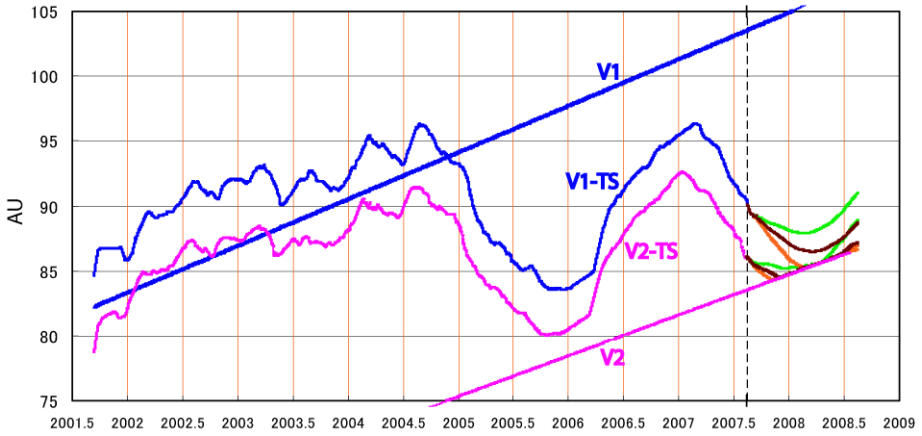

Fig. 12 TS position along the Sun–V1 (*blue*, labeled V1-TS) and Sun–V2 (*pink*, labeled V2-TS) directions based on V2 plasma data from 2001.9.10–2007.8.14 (*dashed vertical line*), together with forecasts for a year after the available V2 plasma data under the assumption that the solar wind ram-pressure is 1.0 (*orange*), 1.25 (*brown*), and 1.5 (*green*) $\times P_{ram,0}$. Note that the TS positions below the V2 line during the forecasting period are not shown. (Washimi et al. 2007b)

the pulse and the reflections at the HP occurring across the whole TS surface. The same is true for the initial increase in R_{TS} because of the solar wind ram-pressure pulse, which also continues for about a year.

Beyond the HP, the transmitted pulse, identified by (c) in Fig. 11, propagates in the interstellar medium at a speed of about 30 km/s. This pulse continues to propagate in the outer heliosheath and will eventually reach the bow shock (BS) (Zank and Müller 2003). In principle, the bow chock will partially reflect the incident wave which could travel back to the HP and further to the TS, affecting the TS position at several tens of years later. However, the damping of waves in the heliosheath makes this unlikely to be an important factor in determining TS and HP location. Another interesting result in Fig. 11 is the formation of a pulse structure at the HP, which splits into 2 humps after ≈ 2 years when the convection pulse arrives at the HP. Because the convection entropy-vorticity modes cannot be transmitted through the HP, these structures accumulate at the HP until, in principle, a steady-state is achieved with an adjusted thermal pressure/magnetic pressure jump across the HP.

A small but finite convection pulse, identified by (d) in Fig. 11, also propagates in the heliosheath. Because the shocked solar wind flow direction in the heliosheath is not radial but is bent poleward, disturbances driven at the TS in lower latitudes are convected to higher latitudes. Consequently, these disturbances cross the sun-V1 line. This speed v_d in Fig. 11 is 130 km/s near the TS and ≈ 14 km/s or less near the HP.

Figure 12 shows the simulated time-varying TS position along the Sun–V1 (blue) and Sun–V2 (pink) trajectories. R_{TS} changes from 84 AU to ≈ 100 AU during the simulation period along the Sun–V1 line. The rapid increases of R_{TS} are due to collisions of ram-pressure pulses with the TS (Washimi et al. 2007a, 2007b). The time-varying TS location along the Sun–V1 line is almost parallel to the V1 trajectory before the V1 crossing. At the end of a series of ram-pressure pulses in October 2004, R_{TS} began to decrease, and V1 crossed the TS in late 2004. R_{TS} continued to decrease rapidly, reaching 84 AU near the end of 2005. This small value of R_{TS} is due to the overshoot discussed above. A maximum in the incoming speed of the TS occurs around 2005.15, and is ≈ 300 km/s, which is almost the

same as speed as the outgoing solar wind. This suggests that the reflected thermal-pressure pulses, which were driven by the series of the strong ram-pressure pulses prior to the V1 crossing, were anomalously strong. After October 2005, the TS started to move out again. At the beginning of this phase, the subsequent increase is rather gradual due to the gradual increase in ram-pressure of the solar wind: these times correspond to solar-minimum when the ram-pressure is relatively high. The increase in R_{TS} is punctuated by a rapid outward acceleration associated with the March 2006 event (Richardson et al. 2006), and R_{TS} reaches a maximum of about 96 AU by the middle of February 2007, then begins to decrease to 90 AU in response to solar wind conditions measured by the most recently available (14 August, 2007) V2 plasma data used in their analysis. Due to the N–S asymmetry of the heliosphere, R_{TS} along the Sun–V2 trajectory is generally less than that along the Sun–V1 line, but the asymmetry is relatively small ($\approx$ 3–6 AU most of the time) and variations in R_{TS} are dominated by temporal solar wind effects. R_{TS} along the Sun–V2 trajectory shows very similar changes when compared to those occurring along the Sun–V1 line. Because the simulation did not include the effects of the neutral interstellar gas, the N–S asymmetry in the Washimi et al. (2007b) simulation is probably overestimated. However, for this low ram-pressure case, R_{TS} along the Sun–V1 line is virtually the same as that along the Sun–V2 trajectory, as illustrated in Fig. 12.

Just before the end of the V2 plasma data, R_{TS} in Fig. 12 begins to decrease. In view of our remarks above concerning reflected heliospheric pulses, this decrease indicated that the TS was moving inward again because of the reflected thermal-pressure pulse associated with the March 2006 event. To quantify this effect, Washimi et al. (2007b) extended the simulation. Because the R_{TS} decrease will continue for at least a year, Washimi et al. forecast the TS location for a year, assuming that the solar wind ram-pressure can take 3 different values, viz., 1.0, 1.25, and 1.5 $\times P_{ram,0}$. As shown in Fig. 12, R_{TS} continued to decrease sharply for all assumed solar wind ram-pressure cases, and R_{TS} was a minimum from October 2007 to March 2008, depending on the assumed ram pressure. The Washimi et al. (2007b) simulations suggested that if the solar wind ram-pressure was 1.0 or 1.25 $\times$ $P_{ram,0}$, a V2-TS crossing would occur in October or November 2007. Rather remarkably, the crossing of the V2 occurred several times between 30 August and 1 September 2007 (Stone et al. 2008; Burlaga et al. 2008; Richardson et al. 2008), which was within a month of the predicted crossing by Washimi et al. (2007b).

A simple nose-cone-type of outer heliospheric model of the kind used by Washimi et al. (2007a, 2007b) will be asymmetric or modified by several possible effects. The ideal MHD simulation of Washimi et al. (2007b) introduces a N-S asymmetry by taking into account the possibility of an obliquely oriented ISMF that is consistent with the HDP observations (Lallement et al. 2005). The response of the TS to the returned pulse reflected at the HP was included properly in the simulations. However, there should certainly be additional effects such as the coupling of neutral H atoms to the plasma, possible anisotropy of the solar wind, and nonlinear magnetic field effects that will contribute to the asymmetry (or absence) of the heliosphere. Besides contributing to the basic symmetrization of the heliosphere, as discussed already, neutral H will introduce slightly different propagation characteristics into both the transmitted waves and shocks in the heliosheath as well as the HP reflected pulses. The solar wind ram pressure anisotropy during solar minimum observed by Ulysses (Phillips et al. 1995; McComas et al. 1999, 2000) will introduce a latitudinal asymmetry in the TS position (Pauls and Zank 1996; Tanaka and Washimi 1999). However, the latitudinal asymmetry is offset somewhat by the presence of neutral H since, as shown by Pauls and Zank (1997a, 1997b), the smaller filtration at higher latitudes results in a greater deceleration of the high latitude solar wind flow

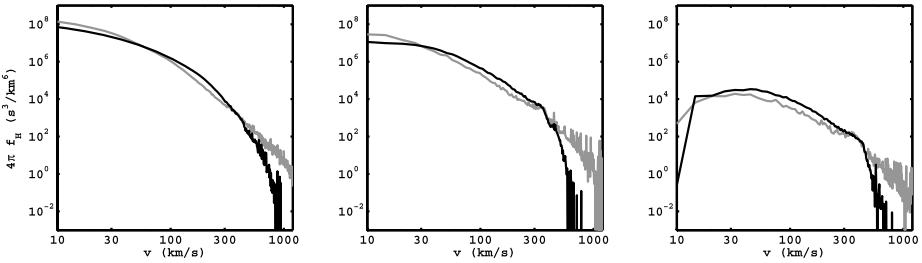

Fig. 13 Velocity distributions of ENA's at three locations along the axis defined by the LISM flow vector with the Sun at the origin: −400 AU in the heliotail (*left*), 180 AU upstream in the hydrogen wall (*middle*), 600 AU in the nearby LISM (*right*). The *black line* is for ENA's obtained from a Maxwellian distribution of heliosheath ions (the parent population of ENA's), and the *gray line* is from a $\kappa = 1.63$ distribution for heliosheath protons in the same steady-state configuration. For small κ fewer medium energy ENA's are present, but more result at low and high energies, which is consistent with the distributions shown in Fig. 1. (Heerikhuisen et al. 2008a)

and an overall isotropization of the solar wind ram pressure throughout the heliosphere. Tanaka and Washimi (1999) also suggested a "dipped" heliospheric structure around the equator which could result in an earlier crossing for V2 than V1, even within a purely MHD model. Thus, additional effects that might modify the predicted V2 crossing distance and time by Washimi et al. (2007b) include both the effect of a time-delay due to neutral particles modifying propagation speeds and the effects of an anisotropic solar wind ram pressure and/or nonlinear magnetic field effects. Nonetheless, the ideal MHD-only forecast of the TS crossing by V2 was remarkably accurate, with the predicted crossing time only in error from that observed by a few months.

A more elaborate multi-fluid model that includes neutral H self-consistently is under development Washimi et al. (2007b).

5 Energetic Neutral Atoms (ENAs)

The use of an isotropic κ-distribution (10) (Fig. 1) to describe the heliospheric plasma has important implications for both the global structure of the heliosphere and the properties and characteristics of the ENA distributions. Heerikhuisen et al. (2008a) discuss the effects of κ-distributed neutral atoms originating from the heliosheath on the global heliosphere-interstellar medium structure, and compute ENA spectra and skymaps. Figure 13 shows the velocity distribution of heliosheath hydrogen at various locations along the LISM flow vector. It is clear from this figure that for a $\kappa = 1.63$ distribution, significantly more H-atoms with energies above 1 keV result than for a Maxwellian ion population in the heliosheath. It is also important to note that ENAs in the heliotail (left plot) show a clear power-law tail ($\sim v^{-5}$), mirroring the plasma, when a κ-distribution is assumed for heliosheath protons. These tails persist even outside the heliosphere (middle and right plots) for energies above 1 keV.

Figure 14 compares plasma density and temperature along radial lines in the nose, polar and tail directions for the Maxwellian and equilibrated $\kappa = 1.63$ heliosheath cases. Secondary charge-exchange of neutrals created in the hot heliosheath was identified by Zank et al. (1996b) as a critical mechanism for the anomalous transport of energy from the shocked solar wind to the shocked and unshocked LISM. In particular, the upwind region abutting the HP experiences considerable heating as a result of secondary charge-exchange of hot

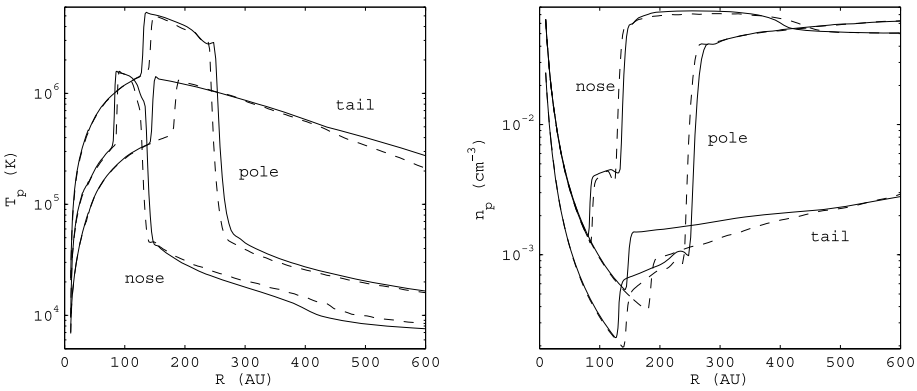

Fig. 14 Radial profiles of effective plasma temperature (*left*) and density (*right*) in the nose, polar (i.e. in the meridional plane), and tail directions. The *solid line* represents the values obtained by using a Maxwellian distribution function for the proton distribution. The *dashed line* is obtained by assuming that the proton distribution in the supersonic and subsonic solar wind can be described as an isotropic κ-distribution with $\kappa = 1.63$. (Heerikhuisen et al. 2008a)

($\sim 10^6$ K) neutrals with the cold LISM protons. The efficiency of this mechanism of anomalous heat transfer is increased with a κ-distribution in the inner heliosheath, resulting simultaneously in a shrinking of the inner heliosheath and an expansion of the outer heliosheath. The inner heliosheath plasma temperature (defined in terms of pressure) remains unchanged, because the Maxwellian and κ-distributions have the same second moment. Heerikhuisen et al. find that the TS moves out by about 4 AU in the nose direction, and the HP moves inward by about 9 AU. The bow shock stand-off distance increases by 25 AU, and the shock itself is weakened by the additional heating of the LISM plasma by fast neutrals from the solar wind. For the anticipated crossing of the HP by the V1 and V2 spacecraft, it is important to note that the inner heliosheath thickness shrinks from 56 AU (Maxwellian plasma distribution based description) to 44 AU (κ plasma distribution), a reduction of nearly 20%. This would reduce the expected V1 crossing time by as much as 3 years.

The filtration rate of hydrogen changes at the HP for a Maxwellian compared to a κ-distribution based model. For the Maxwellian case, the hydrogen density at the TS is about 63% of the interstellar value, whereas the density drops slightly to 60% for the κ-distribution model.

Figure 15 shows three energy spectra for ENA's originating from the nose, tail and polar directions. To obtain these spectra, Heerikhuisen et al. divide the flux measured at 1 AU by the survival probability for each energy band to undo the ionization losses. For the three directions considered, the energy spectrum tends toward the value of -κ above about 1 keV. This result shows that the IBEX data, in spite of being line-of-sight integrated, should be able to determine the spectral slope of the heliosheath protons in the 0.01–6 keV range. Figure 15 also shows that the spectra in the three directions considered have very similar properties. This will not necessarily be true for the real heliosphere, where the post-shock solar wind may develop different high energy tails in different directions. The dotted line (labeled "nose2") is for a spectrum in the nose direction obtained using 32 energy bins (compared to about 10 non-overlapping IBEX bins). The agreement between this curve and the green markers shows that, for $\kappa = 1.63$ at least, the number of IBEX bins is sufficient to reproduce the spectrum.

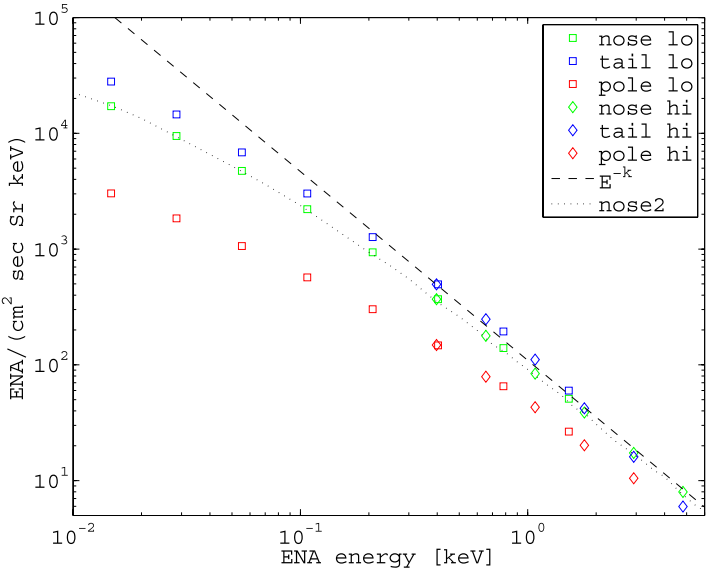

Fig. 15 ENA energy spectra as observed at 1 AU along various lines of sight. The *squares* and *diamonds* represent data using approximate IBEX energy bins obtained by dividing the IBEX-lo and IBEX-hi energy ranges (0.01–2.0 keV and 0.3–6 keV) into 8 and 6 equal bins on a logarithmic scale (see also Prested et al. 2007). The *dotted line* was obtained using narrower bins (32 total), and demonstrates that the IBEX bin widths are sufficiently narrow to maintain accuracy. The *dashed line* has a slope of -κ, which represents the plasma spectrum at a particular point, and appears reasonably well reproduced along the lines of sight considered. (Heerikhuisen et al. 2008a)

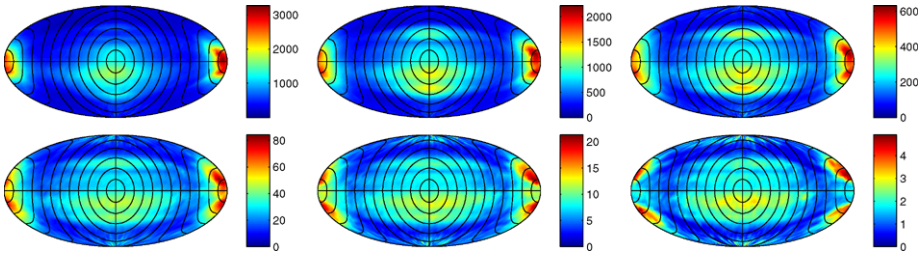

Fig. 16 All-sky maps of ENA flux at 1 AU, in units of $(\mathrm{cm}^2\,\mathrm{Sr\,keV\,sec})^{-1}$, generated in the inner heliosheath through charge-exchange between an interstellar neutral atom and a heliosheath proton drawn from a κ-distribution with $\kappa = 1.63$. The direction of the interstellar flow is at the center of the plot, with the poles top and bottom, and the heliotail on the far sides. *Contour lines* have been drawn at 15° intervals. Maps are generated by binning ENAs, which intersect the 1 AU sphere on radially inward trajectories. The maps from top left to bottom right correspond to the following energies and bin-widths (in eV): 10 ± 2, 50 ± 10, 200 ± 20, 1000 ± 100, 2400 ± 200, and 6000 ± 400. (Heerikhuisen et al. 2008a)

Heerikhuisen et al. (2007) used a steady-state heliosphere to compute all-sky ENA maps. They follow the same procedure for a κ-distribution based model, obtaining ENA's up to several keV in energy. Figure 16 shows all-sky ENA maps obtained from their steady-state solution with a κ distribution for heliosheath protons. The top right plot shows the ENA map for 200 eV, which can be compared with their previous work (Heerikhuisen et al. 2007), where they did not self-consistently couple the plasma and kinetic neutral atoms, and as-

sumed a Maxwellian proton distribution. In the case of a κ-distribution, the ENA flux at 200 eV is two to three times smaller than for the Maxwellian case because more protons are found in the wings of the distribution for a κ-distribution. The decrease of medium energy (100s of eV) ENAs is compensated by an increased ENA flux above 1 keV, and Heerikhuisen et al. (2008a) find a count rate of about 3 atoms per (cm^2 sr s keV) at 6 keV.

Heerikhuisen et al. (2008a) assumed "solar minimum" conditions, with clearly defined high speed wind originating at the poles. The high speed wind creates hotter heliosheath plasma, which in turn increases the energy of ENAs generated in the subsonic polar solar wind. The all-sky maps of Fig. 16 show that at energies above about 1 keV, these streams of hot solar wind dominate the ENA flux, while at lower energies the central tail region is the major source of ENAs. Figure 16 compares skymaps at different energies, showing that the qualitative properties do not vary widely over the IBEX energy range. This contrasts sharply with the results for a Maxwellian heliosheath (Heerikhuisen et al. 2007), where more flux generally come from the tail than the nose at low energies, and the reverse at high energies. This is easily understood from the fewer particles that are found in the wings of the Maxwellian distribution, compared to the much broader κ-distribution. Thus, the relatively cool plasma in the distant heliotail can still be a significant source of high energy ENAs, if we assume it has a κ-distribution.

Acknowledgements The authors acknowledge the partial support of NASA grants NNG04GF83G, NNG05GH38G, NNG05GM62G, NNG05GH48G, NNG06GD43G, and NSF grants ATM0317509, and ATM0428880.

We acknowledge the use of the solar-wind data from the MIT plasma experiment on V2 during the period from day of year 253, 2001 to 226, 2007, for our simulations.

Supercomputer time allocations were provided by the NASA High-End Computing program, DOE's INCITE project PSS001, NCSA project MCA07S033, and by collaborative agreement with the Solar-Terrestrial Environment Laboratory of Nagoya University. Numerical computations were also carried out on the SX-8 machine at the National Institute of Computer Technology in Japan.

References

D. Alexashov, V. Izmodenov, Kinetic vs. multi-fluid models of H atoms in the heliospheric interface: a comparison. Astron. Astrophys. **439**, 1171–1181 (2005)

W.I. Axford, The interaction of the solar wind with the interstellar medium. Solar Wind, NASA Spec. Publ. **SP-308**, 609 (1972)

W.I. Axford, A.J. Dessler, B. Gottlieb, Astrophys. J. **137**, 1268 (1963)

S.J. Bame, J.R. Asbridge, H.E. Felthauser, E.W. Hones, I.B. Strong, J. Geophys. Res. **72**, 113 (1967)

V.B. Baranov, Y.G. Malama, J. Geophys. Res. **98**, 15157 (1993)

V.B. Baranov, Y.G. Malama, J. Geophys. Res. **100**, 14755 (1995)

V.B. Baranov, K. Krasnobaev, A. Kulikovsky, Sov. Phys. Dokl. **15**, 791 (1971)

V.B. Baranov, M.K. Ermakov, M.G. Lebedev, Three-component gasdynamic model of the interaction of the solar wind with the interstellar medium. Sov. Astron. Lett. **7**, 206 (1981)

T. Borrmann, H. Fichtner, Adv. Space Sci. **35**, 2091 (2005)

S.N. Borovikov, J. Heerikhuisen, N.V. Pogorelov, I.A. Kryukov, G.P. Zank, in *Numerical Modeling of Space Plasma Flows: ASTRONUM-2007*, ed. by N.V. Pogorelov, E. Audit, G.P. Zank (ASP, San Francisco, 2008a), pp. 197–203

S.N. Borovikov, N.V. Pogorelov, G.P. Zank, I.A. Kryukov, Astrophys. J. **682**, 1404 (2008b)

J.M. Burgers, *Flow Equations for Composite Gases* (Academic Press, New York, 1969)

L.F. Burlaga et al., Science **309**, 2027–2029 (2005)

L.F. Burlaga et al., Nature **454**, 75 (2008)

M.R. Collier, Geophys. Res. Lett. **22**, 2673 (1995)

D.P. Cox, L. Helenius, Flux-tube dynamics and a model for the origin of the Local Fluff. Astrophys. J. **583**, 205 (2003)

A. Dalgarno, Proc. Phys. Soc. **75**, 374 (1960)

L.E. Davis, Interplanetary magnetic fields and cosmic rays. Phys. Rev. **100**, 1440 (1955)
R.B. Decker et al., Science **309**, 2020 (2005)
R.B. Decker et al., Nature **454**, 67 (2008)
H.J. Fahr, S. Grzedzielski, R. Ratkiewicz, Ann. Geophys. **6**, 337 (1988)
H.J. Fahr, T. Kausch, H. Scherer, Astron. Astrophys. **357**, 268 (2000)
L.A. Fisk, G. Gloeckler, Astrophys. J. **640**, L79 (2006)
W.L. Fite, A.C.H. Smith, R.F. Stebbings, Charge transfer in collisions involving symmetric and asymmetric resonance. Proc. R. Soc. Lond. Ser. A **268**, 527 (1962)
V. Florinski, G.P. Zank, N.V. Pogorelov, J. Geophys. Res. **108**(A6), 1228 (2003a). doi:10.1029/2002JA009695
V. Florinski, G.P. Zank, Comment on "On nonideal MHD properties of the partially ionized interstellar gas" by V.B. Baranov and H.J. Fahr. J. Geophys. Res. **108**(A12), 1438 (2003d). doi:10.1029/2003JA009950
V. Florinski, G.P. Zank, The galactic cosmic ray intensity in the heliosphere in response to variable interstellar environments, in *Solar Journey: The Significance of Our Galactic Environment for the Heliosphere and Earth*, ed. by P.C. Frisch (Springer, Netherlands, 2006), p. 281
V. Florinski, G.P. Zank, W.I. Axford, The solar system in a dense interstellar cloud: implications for cosmic ray fluxes at Earth and 10Be records. Geophys. Res. Lett. **30**, 2206 (2003b). doi:10.1029/2003GL017566
V. Florinski, N.V. Pogorelov, G.P. Zank, B.E. Wood, D.P. Cox, Astrophys. J. Lett. **604**, 700 (2004a)
V. Florinski, G.P. Zank, N.V. Pogorelov, J. Geophys. Res. (Space), **110**(A7) (2005a). CiteID A07104
P.C. Frisch, Characteristics of nearby interstellar matter. Space Sci. Rev. **72**, 499 (1995)
G.P. Gayley, G.P. Zank, H.L. Pauls, P.C. Frisch, D.E. Welty, One-shock or two-shock heliosphere: Lyman-α observations and measurements. Astrophys. J. **487**, 259 (1997)
G. Gloeckler, Space Sci. Rev. **78**, 335 (1996)
G. Gloeckler, J. Geiss, Space Sci. Rev. **86**, 127 (1998)
G. Gloeckler, J. Geiss, H. Balsiger, L.A. Fisk, A.B. Galvin, F.M. Ipavich, K.W. Ogilvie, R. von Steiger, B. Wilken, Detection of interstellar pick-up hydrogen in the solar system. Science **261**, 70 (1993)
D.A. Gurnett, W.S. Kurth, Electron plasma oscillations upstream of the solar wind termination shock. Science **309**, 2025–2027 (2005)
D.A. Gurnett, W.S. Kurth, Nature **454**, 67 (2008)
J. Heerikhuisen, V. Florinski, G.P. Zank, Interaction between the solar wind and interstellar gas: a comparison between Monte-Carlo and fluid approaches, J. Geophys. Res. **111**(A6) (2006). CiteID A06110
J. Heerikhuisen et al., in *Numerical Modeling of Space Plasma Flows: ASTRONUM-2006*, ed. by N.V. Pogorelov. ASP Conf., vol. 359 (Astronomical Society of the Pacific, San Francisco, 2006b), p. 251
J. Heerikhuisen, N.V. Pogorelov, G.P. Zank, V. Florinski, Astrophys. J. **655**, L53 (2007)
J. Heerikhuisen, N.V. Pogorelov, V. Florinski, G.P. Zank, J. le Roux, Astrophys. J. **682**, 679 (2008a)
J. Heerikhuisen et al., in *Numerical Modeling of Space Plasma Flows: ASTRONUM-2008*, ed. by N.V. Pogorelov, E. Audit, G.P. Zank. ASP Conf. Ser. (Astronomical Society of the Pacific, San Francisco, 2008b)
P.A. Isenberg, Interaction of the solar wind with interstellar neutral hydrogen: Three-fluid model. J. Geophys. Res. **91**, 9965 (1986)
P.A. Isenberg, W.C. Feldman, Electron-impact ionization of interstellar hydrogen and helium at interplanetary shocks. Geophys. Res. Lett. **22**, 873 (1995)
P.A. Isenberg, M.A. Lee, A dispersive analysis of bispherical pickup ion distributions. J. Geophys. Res. **101**(11), 055 (1996)
P.A. Isenberg, C.W. Smith, W.H. Matthaeus, Turbulent heating of the distant solar wind by interstellar pickup protons. Astrophys. J. **592**, 564–573 (2003)
V.V. Izmodenov, J. Geiss, R. Lallement, G. Gloeckler, V.B. Baranov, Y.G. Malama, Filtration of interstellar hydrogen in the two-shock heliospheric interface: Inferences on the local interstellar cloud electron density. J. Geophys. Res. **104**, 4731 (1999)
V.V. Izmodenov, D. Alexashov, A. Myasnikov, Astron. Astrophys. **437**, L35–L38 (2005)
J.R. Jokipii, J. Giacalone, Astrophys. J. **605**, L145–L148 (2004)
J.R. Jokipii, J. Giacalone, J. Kota, **611**, L141–L144 (2004)
S.R. Karmesin, P.C. Liewer, J.U. Brackbill, Geophys. Res. Lett. **22**, 1153 (1995)
I.K. Khabibrakhmanov, D. Summers, G.P. Zank, H.L. Pauls, Solar wind flow with interstellar hydrogen pickup. Astrophys. J. **469**, 921 (1996)
R.M. Kulsrud, in *Basic Plasma Physics*, ed. by A.A. Galeev, R.N. Sudan. vol. 1 (North Holland Publ., Amsterdam, 1984), p. 115
R. Lallement, E. Quemerais, J.L. Bertaux, S. Ferron, D. Koutroumpa, R. Pellinen, Science **307**, 1447 (2005)
P.C. Liewer, S.R. Karmesin, J.U. Brackbill, Hydrodynamic instability of the heliopause driven by plasma-neutral charge-exchange interactions. J. Geophys. Res. **101**, 17119 (1996)

T. Linde, T.I. Gombosi, P.L. Roe, K.G. Powell, D.L. DeZeeuw, The heliosphere in the magnetized local interstellar medium: results of a 3D MHD simulation. J. Geophys. Res. **103**, 1889 (1998)
B.J. Lindsay, R.F. Stebbings, J. Geophys. Res. **110**, A12213 (2005)
J.L. Linsky, B.E. Wood, The α Cen line of sight: D/H ratio, physical properties of local interstellar gas, and measurement of heated hydrogen near the heliopause. Astrophys. J. **463**, 254 (1996)
A.S. Lipatov, G.P. Zank, H.L. Pauls, The interaction of neutral interstellar *H* with the heliosphere: A2.5D particle-mesh Boltzmann simulation. J. Geophys. Res. **103**, 20,631 (1998)
L. Maher, B. Tinsley, Atomic hydrogen escape rate due to charge exchange with hot plasmaspheric ions. J. Geophys. Res. **82**, 689 (1977)
Yu.G. Malama, Monte-Carlo simulation of neutral atoms trajectories in the solar system. Astrophys. Space Sci. **176**, 21 (1991)
W.H. Matthaeus, G.P. Zank, C.W. Smith, S. Oughton, Turbulence, spatial transport, and heating of the solar wind. Phys. Rev. Lett. **82**, 3444 (1999)
D.J. McComas, H.O. Funsten, J.T. Gosling, W.R. Pryor, ULYSSES measurements of variations in the solar wind-interstellar hydrogen charge exchange rate. Geophys. Res. Lett. **26**(17), 2701 (1999)
D.J. McComas, B.L. Barraclough, H.O. Funsten, J.T. Gosling, E. Santiago-Muñoz, R.M. Skoug, B.E. Goldstein, M. Neugebauer, P. Riley, A. Balogh, Solar wind observations over Ulysses' first full polar orbit. J. Geophys. Res. **105**, 10419 (2000)
D.J. McComas, F. Allegrini, L. Bartolone, P. Bochsler, M. Bzowski, M. Collier, H. Fahr, H. Fichtner, P. Frisch, H. Funsten, S. Fuselier, G. Gloeckler, M. Gruntman, V. Izmodenov, P. Knappenberger, M. Lee, S. Livi, D. Mitchell, E. Möbius, T. Moore, S. Pope, D. Reisenfeld, E. Roelof, H. Runge, J. Scherrer, N. Schwadron, R. Tyler, M. Wieser, M. Witte, P. Wurz, G. Zank, The Interstellar Boundary Explorer (IBEX): Update at the end of phase B, in *The Physics of the Inner Heliosheath*, ed. by J. Heerikhuisen, V. Florinski, G.P. Zank, AIP Conference Proceedings, vol. 858 (2006), pp. 241–250
F.B. McDonald, E.C. Stone, A.C. Cummings, B. Heikkila, N. Lal, W.R. Webber, Nature **426**, 48 (2003)
J.F. McKenzie, K.O. Westphal, Phys. Fluids **11**, 2350 (1968)
R.A. Mewaldt et al., in Joint SOHO/ACE workshop "Solar and Galactic Composition, ed. by R.F. Wimmer-Schweingruber. American Institute of Physics Conference Series, vol. 598 (2001), p. 165
E. Möbius, D. Hovestadt, B. Klecker, M. Scholer, G. Gloeckler, Nature **318**, 426 (1985)
E. Möbius, M. Bzovski, S. Chalov, H.-J. Fahr, G. Gloeckler et al., Astron. Astrophys. **426**, 897 (2004)
H.-R. Müller, P.C. Frisch, G.P. Zank, Astrophys. J. **647**(2), 1491 (2006)
M. Opher, E.C. Stone, P.C. Liewer, Astrophys. J. **640**, L71 (2006)
E.N. Parker, Dynamics of interplanetary gas and magnetic fields. Astrophys. J. **123**, 644 (1958)
E.N. Parker, The stellar-wind regions. Astrophys. J. **134**, 20 (1961)
E.N. Parker, *Interplanetary Dynamical Processes* (Interscience, New York, 1963)
H.L. Pauls, G.P. Zank, Interaction of a nonuniform solar wind with the local interstellar medium. J. Geophys. Res. **101**, 17081 (1996)
H.L. Pauls, G.P. Zank, Interaction of a nonuniform solar wind with the local interstellar medium. 2. A two-fluid model. J. Geophys. Res. **102**, 19,779 (1997a)
H.L. Pauls, G.P. Zank, Modelling the solar wind/interstellar wind interaction, in *Proc. 25th Int. Cosmic Ray Conf.*, vol. 2 (1997b), p. 241
H.L. Pauls, G.P. Zank, L.L. Williams, Interaction of the solar wind with the local interstellar medium. J. Geophys. Res. **100**, 21,595 (1995)
Phillips et al., Science **268**, 1030 (1995)
N.V. Pogorelov, T. Matsuda, Nonevolutionary MHD shocks in the solar wind and interstellar medium interaction. Astron. Astrophys. **354**, 697 (2000)
N.V. Pogorelov, A.Y. Semenov, Solar wind interaction with the magnetized interstellar medium. Shock-capturing modeling. Astron. Astrophys. **321**, 330 (1997)
N.V. Pogorelov, G.P. Zank, in *Numerical Modeling of Space Plasma Flows*, ed. by N.V. Pogorelov, G.P. Zank. ASP Conf. Ser., vol. 359 (ASP, San Francisco, 2006), p. 184
N.V. Pogorelov, G.P. Zank, T. Ogino, Three-dimensional features of the outer heliosphere due to coupling between the interstellar and interplanetary magnetic fields I. Magnetohydrodynamic model: interstellar perspective. Astrophys. J. **614**, 1007 (2004)
N.V. Pogorelov, G.P. Zank, T. Ogino, Astrophys. J. **644**, 1299 (2006)
N.V. Pogorelov, E.C. Stone, V. Florinski, G.P. Zank, Astrophys. J. **668**, 611 (2007)
N.V. Pogorelov, J. Heerikhuisen, G.P. Zank, Astrophys. J. **675**, L41 (2008a)
N.V. Pogorelov, J. Heerikhuisen, G.P. Zank, S.N. Borovikov, Space Sci. Rev. (2008)
N.V. Pogorelov, G.P. Zank, S.N. Borovikov, V. Florinski, J. Heerikhuisen, I.A. Kryukov, in *Numerical Modeling of Space Plasma Flows: ASTRONUM-2007*, ed. by N.V. Pogorelov, E. Audit, G.P. Zank. ASP Conf. Ser., vol. 385 (Astronomical Society of the Pacific, San Francisco, 2008b), pp. 180–188

N.V. Pogorelov et al., in *Particle Acceleration in the Heliosphere and Beyond*, ed. by Gang Li, Qiang Hu, and G.P. Zank, AIP Conference Proceedings (2008c)
C. Prested et al., J. Geophys. Res. (2007, accepted)
C. Prested, N. Schwadron, J. Passuite, B. Randol, B. Stuart, G. Crew, J. Heerikhuisen, N. Pogorelov, G. Zank, M. Opher, F. Allegrini, D.J. McComas, M. Reno, E. Roelof, S. Fuselier, H. Funsten, E. Moebius, L. Saul, Implications of solar wind suprathermal tails for IBEX ENA images of the heliosheath. J. Geophys. Res. **113**(A6), (2008)
R. Ratkiewicz, A. Barnes, G.A. Molvik, J.R. Spreiter, S.S. Stahara, M. Vinokur, S. Venkateswaran, Effect of varying strength and orientation of local interstellar magnetic field on configuration of exterior heliosphere: 3D MHD simulations. Astron. Astrophys. **335**, 363 (1998)
J.D. Richardson, C. Wang, M. Zhang, in 5th *International IGPP Conf.* AIP Conf. Proc., vol. 85 (2006). p. 110
J.D. Richardson et al., Nature **454**, 63 (2008)
H.L. Ripken, H.J. Fahr, Astron. Astrophys. **122**, 181 (1983)
K. Scherer, H. Fichtner, O. Stawicki, The heliosphere, cosmic rays, climate, in *The Outer Heliosphere: The next Frontiers*, ed. by K. Scherer, H. Fichtner, H.-J. Fahr, E. Marsch (Pergamon, New York, 2001), p. 493
K. Scherer, H.J. Fahr, Geophys. Res. Lett. **30**(2), 1045 (2003)
K. Scherer, H. Fichtner, B. Heber, S.E.S. Ferreira, M.S. Potgieter, Adv. Space Res. **41**(8), 1171 (2008)
J.D. Slavin, P.C. Frisch, The ionization of nearby gas. Astrophys. J. **565**, 364 (2002)
C.W. Smith, W.H. Matthaeus, G.P. Zank, N.F. Ness, S. Oughton, J.D. Richardson, Heating of the low-latitude solar wind by dissipation of turbulent magnetic fluctuations. J. Geophys. Res. Space **106**, 8253–8272 (2000)
E.C. Stone et al., Science **309**, 2017 (2005)
E.C. Stone et al., Nature **454**, 71 (2008)
D. Summers, R.M. Thorne, Phys. Fluids B **3**, 1835 (1991)
T. Tanaka, H. Washimi, J. Geophys. Res. **104**, 12605 (1999)
C. Wang, J.W. Belcher, Numerical investigation of hydrodynamic instabilities of the heliopause. J. Geophys. Res. **103**, 247 (1998)
H. Washimi, T. Tanaka, 3-D magnetic field and current system in the heliosphere. Space Sci. Rev. **78**, 85 (1996)
H. Washimi, T. Tanaka, Adv. Space Res. **27**, 509 (2001)
H. Washimi, G.P. Zank, T. Tanaka, *5rd International IGPP Conf.* AIP Conf. Proc. vol. 858 (2006), p. 58
H. Washimi, G.P. Zank, Q. Hu, T. Tanaka, *6th International IGPP Conf.* AIP Proc. vol. 932 (2007a), p. 153
H. Washimi, G.P. Zank, Q. Hu, T. Tanaka, K. Munakata, Astrophys. J. Lett. **670**, L139 (2007b)
L.L. Williams, G.P. Zank, The effect of magnetic field geometry on the wave signature of the pickup of interstellar neutrals. J. Geophys. Res. **99**, 19,229 (1994)
L.L. Williams, G.P. Zank, W.H. Matthaeus, Dissipation of pick-up induced waves: A solar wind temperature increase in the outer heliosphere? J. Geophys. Res. **100**, 17,059 (1995)
L.L. Williams, D.T. Hall, H.L. Pauls, G.P. Zank, The heliospheric Hydrogen distribution: A multi-fluid model. Astrophys. J. **476**, 366 (1997)
M. Witte, Kinetic parameters of interstellar neutral helium. Review of results obtained during one solar cycle with the Ulysses/GAS-instrument. Astron. Astrophys. **426**, 835 (2004)
B.E. Wood, J.L. Linsky, H.-R. Müller, G.P. Zank, Observational estimates for the mass-loss rates of alpha Centauri and Proxima Centauri using HST Ly-alpha spectra. Astrophys. J. Lett. **547**, L49–L52 (2001)
G.P. Zank, Interaction of the solar wind with the local interstellar medium: A theoretical perspective. Space Sci. Rev. **89**, 413 (1999)
G.P. Zank, The dynamical heliosphere, in *Solar Wind Nine*, ed. by S.R. Habbal, R. Esser, J.V. Hollweg, P.A. Isenberg, AIP Conf. Proc., vol. 471 (1999d), pp. 783–786
G.P. Zank, P.C. Frisch, Consequences of a change in the galactic environment of the Sun. Astrophys. J. **518**, 965 (1999e)
G.P. Zank, H.-R. Müller, The dynamical heliosphere. J. Geophys. Res. **108**(A6), 1240 (2003). doi:10.1029/2002JA009689
G.P. Zank, W.H. Matthaeus, C.W. Smith, Evolution of turbulent magnetic fluctuation power with heliospheric distance. J. Geophys. Res. **101**, 17,081 (1996a)
G.P. Zank, H.L. Pauls, I.H. Cairns, G.M. Webb, Interstellar pick-up ions and perpendicular shocks: implications for the termination shock and interplanetary shocks. J. Geophys. Res. **101**, 457 (1996b)
G.P. Zank, H.L. Pauls, L.L. Williams, D.T. Hall, Interaction of the solar wind with the local interstellar medium: A multifluid approach. J. Geophys. Res. **101**(21), 639 (1996d)

G.P. Zank, W.H. Matthaeus, J.W. Bieber, H. Moraal, The radial and latitudinal dependence of the cosmic ray diffusion tensor in the heliosphere. J. Geophys. Res. **103**, 2085 (1998)
G.P. Zank, H.-R. Mueller, V. Florinski, P.C. Frisch, Heliospheric variation in response to changing interstellar environments, in *Solar Journey: Significance of our Galactic Environment for the Heliosphere and Earth*, ed. by G.P. Zank (Springer, Berlin, 2006), p. 23
G.P. Zank et al., Space Sci. Rev. (2008, in preparation)